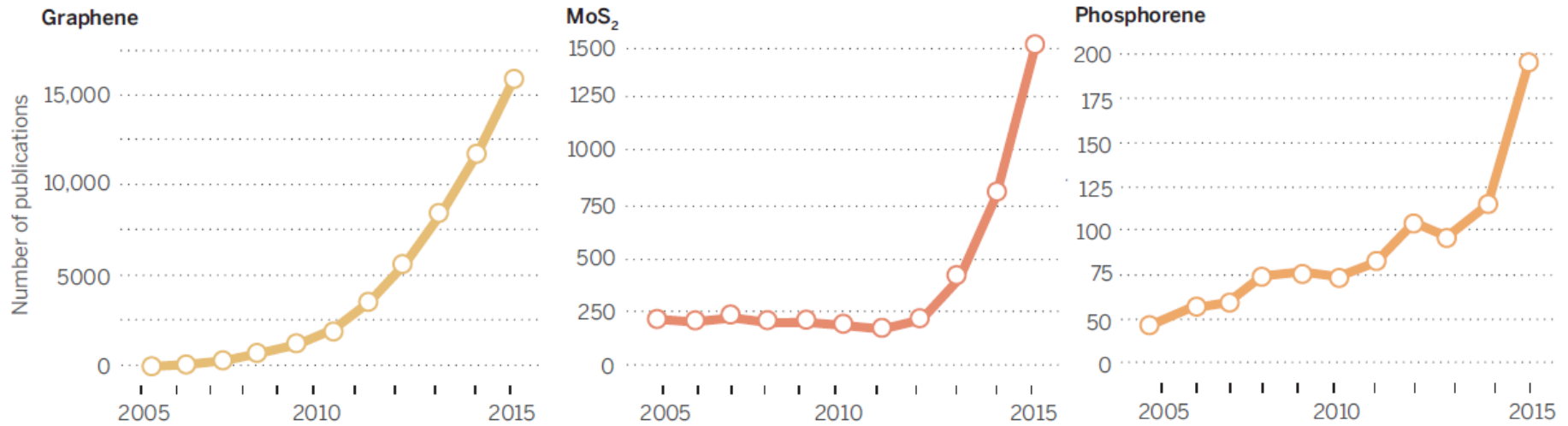


Transition Metal Dichalcogenides
(TMDs)
MoS₂ and more

The rise of the flattest materials

The number of papers on graphene has grown exponentially since the material was isolated in 2004. Publications about molybdenum disulfide (MoS_2) and phosphorene are now repeating the pattern.

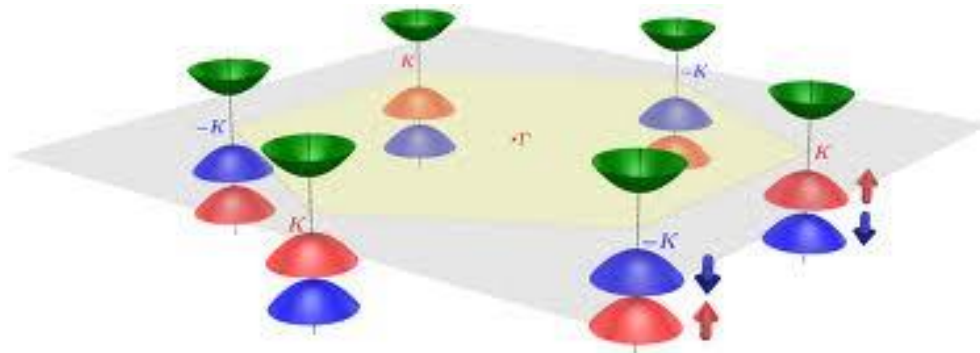


Transition Metal Dichalcogenides (TMDs)

Formula : MX_2 M (transition metals) = Mo, W, Nb, Re, Ti, Ta, etc.
X (chalcogenides) = S, Se, or Te

Semiconducting TMDs

- Semi-metal: TiS_2
- Charge-density-wave (CDW)
- Superconductivity: i.e. MoS_2 Appl. Phys. Lett. 101, 042603 (2012);
- Metal-Insulator Transition (<http://arxiv.org/abs/1301.4947>)
- **Valleytronics**, involves channeling the charge carriers into "valleys" of set momentum in a controlled way.



Motivation

1. Why TMDs?

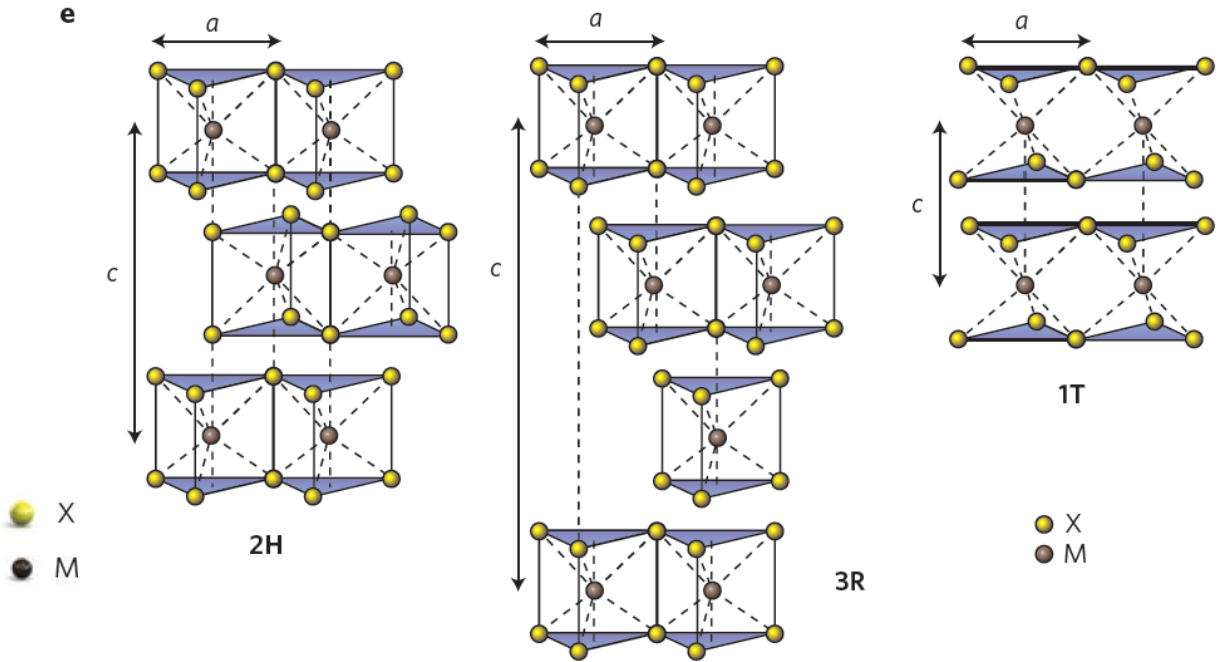
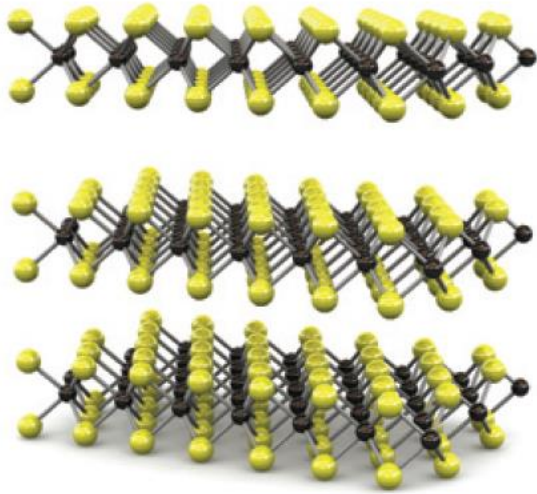
- A 2D semiconducting transition metal dichalcogenides with potential applications that could complement those of Graphene.
 - High on/off ratio and moderate mobility: *electronics*
 - Direct bandgap (for monolayer): *optoelectronics*
 - *Valleytronics*
- *Large area vapor phase growth accessible (so far MoS₂)*

2. Bandgap Engineering

- Layer numbers (quantum confinement)
- Strain
- Temperature
- Potentially leads to many optoelectronics applications.

Introduction: TMDc Monolayer

a

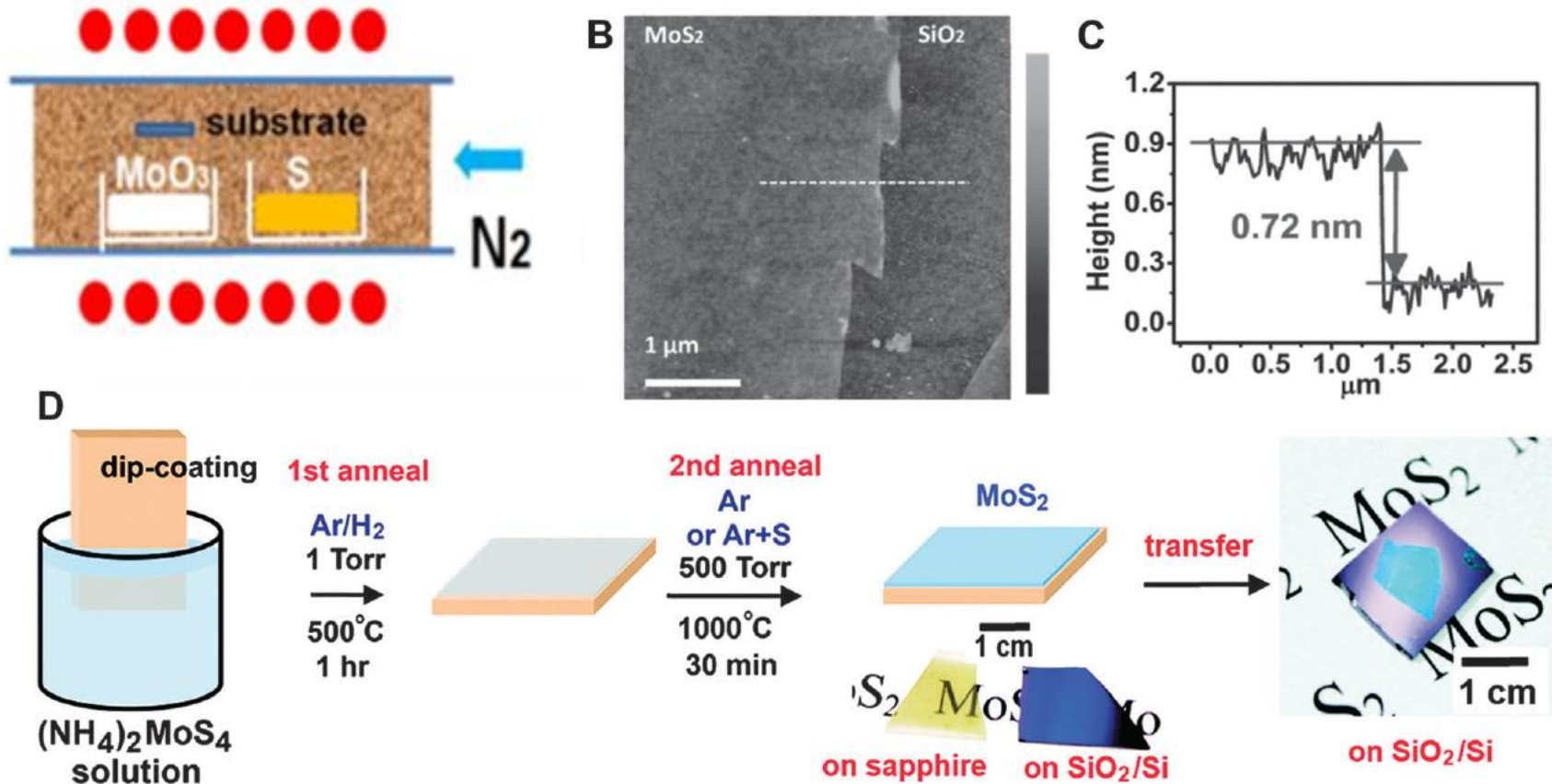


Schematics of the structural polytypes:

- 2H (hexagonal symmetry, two layers per repeat unit, trigonal prismatic coordination),
- 3R (rhombohedral symmetry, three layers per repeat unit, trigonal prismatic coordination), and
- 1T (tetragonal symmetry, one layer per repeat unit, octahedral coordination).

Andras Kis, Nature Nanotech, Vol 6, No 3, 146, (2011).

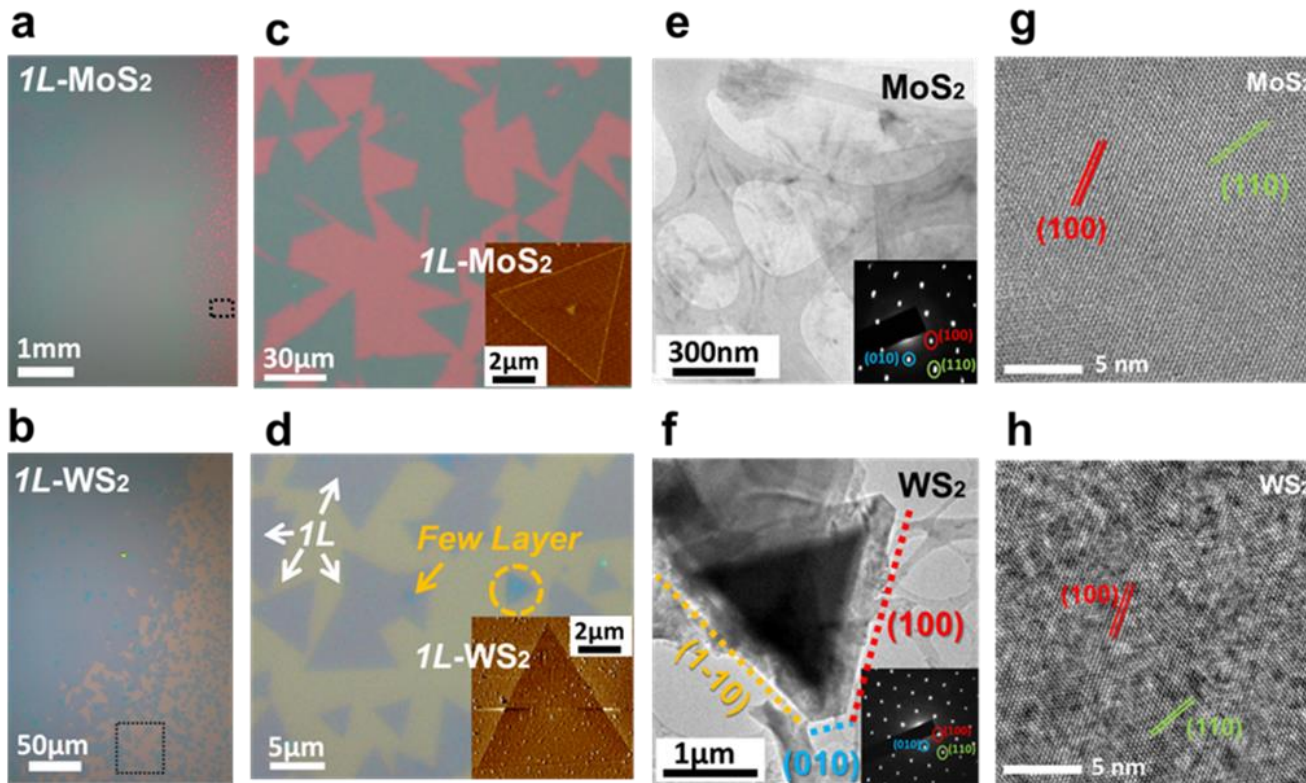
Schematic illustration of the experimental set-up for CVD-growth of MoS₂



Andras Kis, Nature Nanotechnology
Vol 6, No 3, 146, (2011).

Synthesis: the thinnest semiconductors, TMD Monolayer

- Scalable,
- Single Crystal
- Thinnest semiconductors



Synthesis of Single Layer Transition Metal Disulfides on Diverse Surfaces

YHLee et. al., *Nano Lett.* 13, 1852–1857 (2013)

YHLee et. al., *Adv. Mater.* 24, 2320-2325 (2012)

Atomically Thin MoS₂: A New Direct-Gap Semiconductor

K. F. Mak, T. Heinz, PRL 105, 136805 (2010)

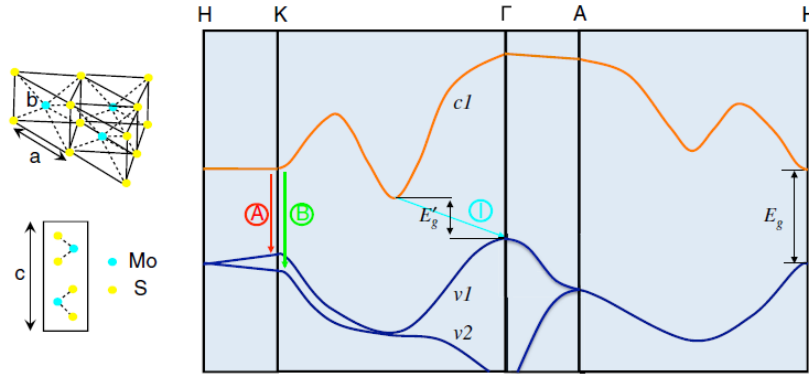


FIG. 1 (color online). Lattice structure of MoS₂ in both the in- and out-of-plane directions and simplified band structure of bulk MoS₂, showing the lowest conduction band $c1$ and the highest split valence bands $v1$ and $v2$. A and B are the direct-gap transitions, and I is the indirect-gap transition. E'_g is the indirect gap for the bulk, and E_g is the direct gap for the monolayer.

- Via optical absorption, photoluminescence, and photoconductivity spectroscopy, the effect of quantum confinement of MoS₂ is traced.
- This leads to a crossover to a direct-gap material in the limit of the single monolayer.
- The freestanding monolayer exhibits an increase in luminescence quantum efficiency by more than a factor of 10^4 compared with the bulk material.

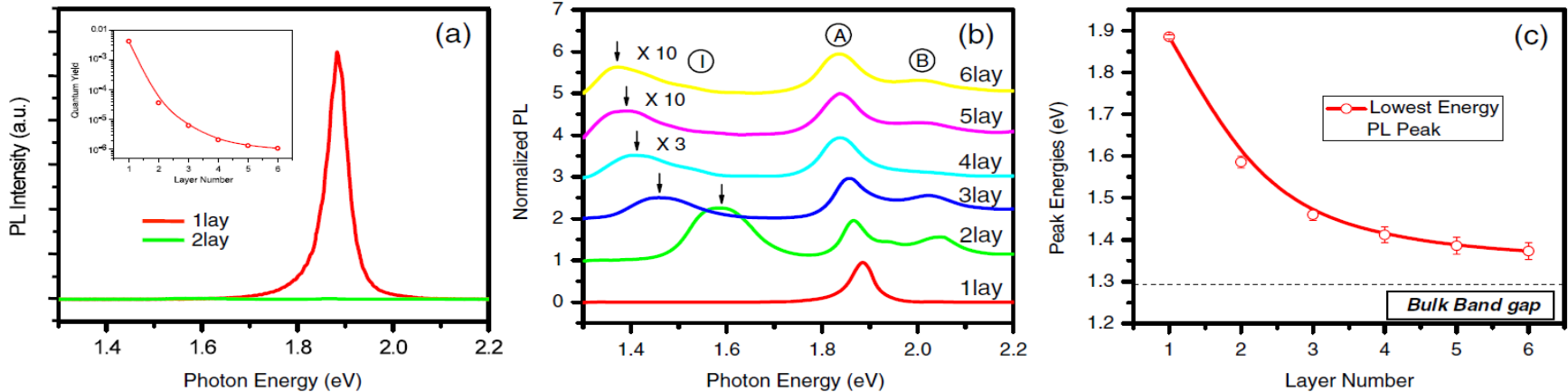
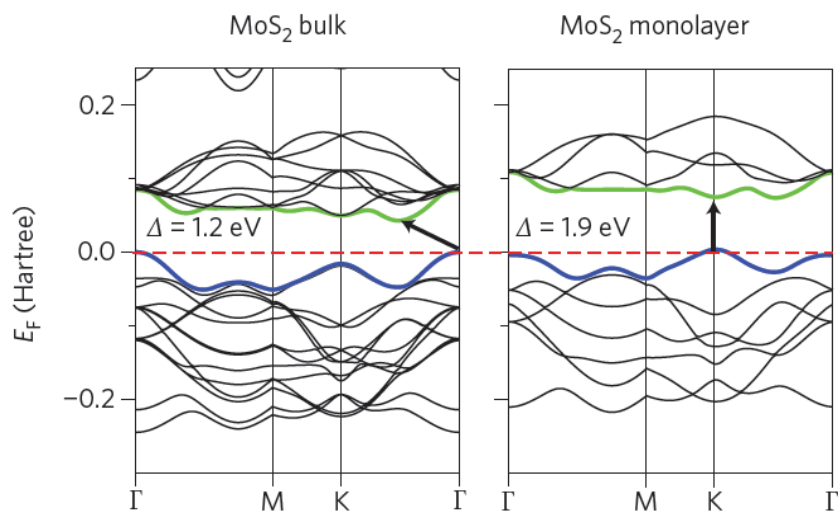
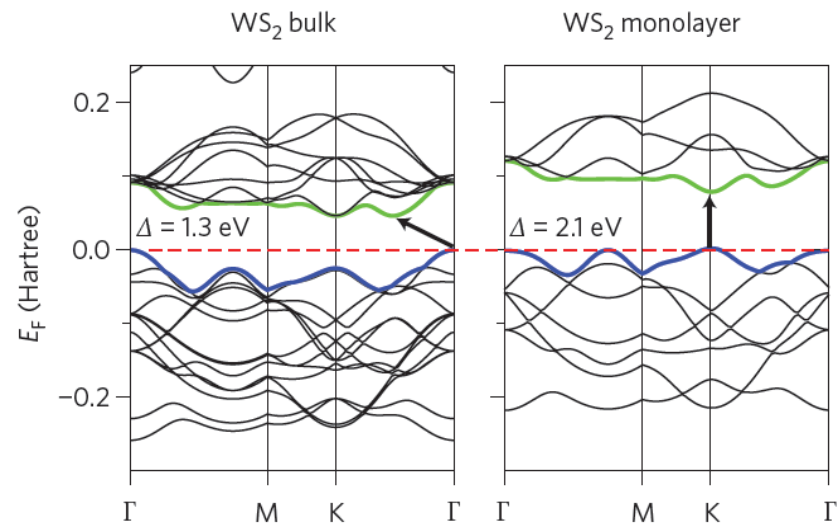


FIG. 3 (color online). (a) PL spectra for mono- and bilayer MoS₂ samples in the photon energy range from 1.3 to 2.2 eV. Inset: PL QY of thin layers for $N = 1-6$. (b) Normalized PL spectra by the intensity of peak A of thin layers of MoS₂ for $N = 1-6$. Feature I for $N = 4-6$ is magnified and the spectra are displaced for clarity. (c) Band-gap energy of thin layers of MoS₂, inferred from the energy of the PL feature I for $N = 2-6$ and from the energy of the PL peak A for $N = 1$. The dashed line represents the (indirect) band-gap energy of bulk MoS₂.

Table 1 | Summary of TMDC materials and properties.

		-S₂		-Se₂		-Te₂	
	Electronic characteristics	References	Electronic characteristics	References	Electronic characteristics	References	
Nb	Metal; superconducting; CDW	138 (E)	Metal; superconducting; CDW	138,164 (E)	Metal	83 (T)	
Ta	Metal; superconducting; CDW	138,164 (E)	Metal; superconducting; CDW	138,164 (E)	Metal	83 (T)	
Mo	Semiconducting 1L: 1.8 eV Bulk: 1.2 eV	31 (E) 88 (E)	Semiconducting 1L: 1.5 eV Bulk: 1.1 eV	82 (T) 88 (E)	Semiconducting 1L: 1.1 eV Bulk: 1.0 eV	82 (T) 165 (E)	
W	Semiconducting 1L: 2.1 eV 1L: 1.9 eV Bulk: 1.4 eV	25 (T) 82 (T) 88 (E)	Semiconducting 1L: 1.7 eV Bulk: 1.2 eV	83 (T) 88 (E)	Semiconducting 1L: 1.1 eV	83 (T)	

Andras Kis, Nature Nanotechnology Vol 6, No 3, 146, (2011).

a**b**

Coupled Spin and Valley Physics in MoS₂

- ❑ Inversion symmetry breaking, together with strong SOC, lead to coupled spin and valley physics in monolayer MoS₂ and other group-VI dichalcogenides, making possible spin and valley control in these 2D materials.
- ❑ **First**, the valley Hall effect is accompanied by a spin Hall effect in both electron-doped and hole-doped systems.
- ❑ **Second**, spin and valley relaxation are suppressed at the valence-band edges, as flip of each index alone is forbidden by the valley-contrasting spin splitting (0.1–0.5 eV) caused by inversion symmetry breaking.
- ❑ **Third**, the valley-dependent optical selection rule also becomes spin-dependent, and carriers with various combination of **valley and spin indices** can be selectively excited by optical fields of different circular polarizations and frequencies.
- ❑ We predict photo-induced charge Hall, spin Hall and valley Hall effects.

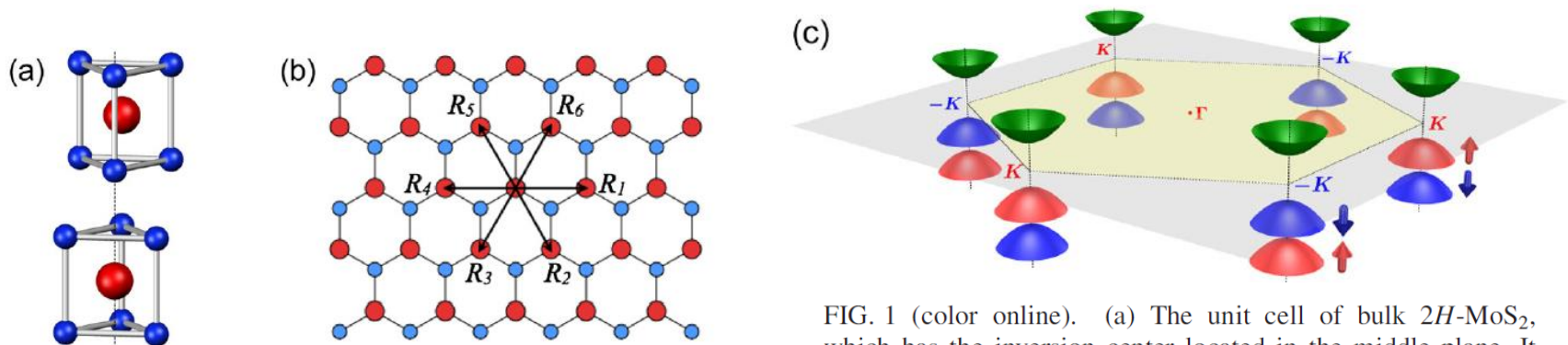
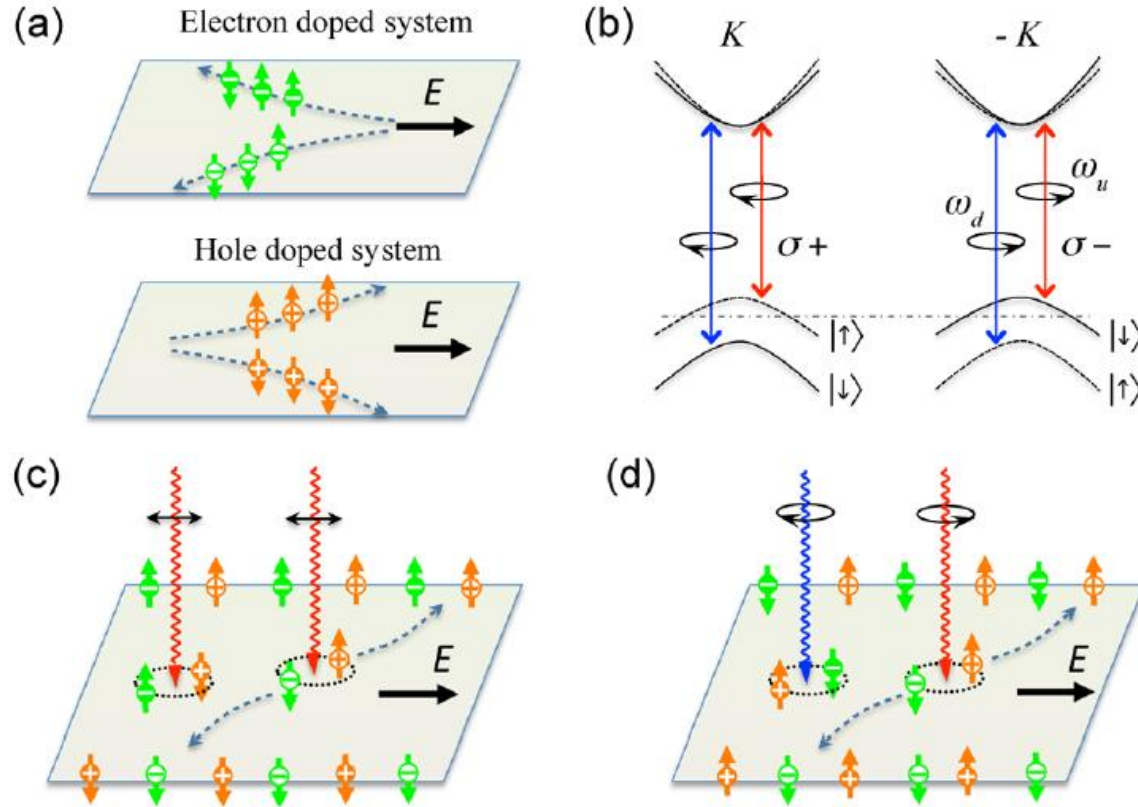


FIG. 1 (color online). (a) The unit cell of bulk 2H-MoS₂, which has the inversion center located in the middle plane. It contains two unit cells of MoS₂ monolayers, which lacks an inversion center. (b) Top view of the MoS₂ monolayer. R_i are the vectors connecting nearest Mo atoms. (c) Schematic drawing of the band structure at the band edges located at the K points.

Photo-induced charge Hall, spin Hall, and valley Hall effects



Coupled spin and valley physics in monolayer group-VI dichalcogenides.

The electrons and holes in valley K are denoted by white '+', and '-' symbol in dark circles and their counterparts in valley $-K$ are denoted by inverse color. (a) Spin Hall effects in electron and hole-doped systems. (b) Valley and spin optical transition selection rules. Solid (dashed) curves denote bands with spin-down (-up) quantized along the out-of-plane direction. The splitting in the conduction band is exaggerated. ω_u and ω_d are, respectively, the transition frequencies from the two split valence-band tops to the conduction band bottom. (c) Spin Hall effects of electrons and holes excited by linearly polarized optical field with frequency ω_u . (d) Valley Hall effects of electrons and holes excited by two-color optical fields with frequencies ω_u and ω_d and opposite circular polarizations.

Superconductivity in MoS_2

- Electro-static carrier doping was attempted in a layered MoS_2 by constructing an electric double-layer transistor with an ionic liquid.
- With the application of gate voltage $V_G > 3\text{V}$, a metallic behavior was observed in the MoS_2 channel.
- An onset of electric field-induced superconductivity was found in the field induced metallic phase. With a maximum T_C of 9.4K.
- APL, 101, 042603 (2012).

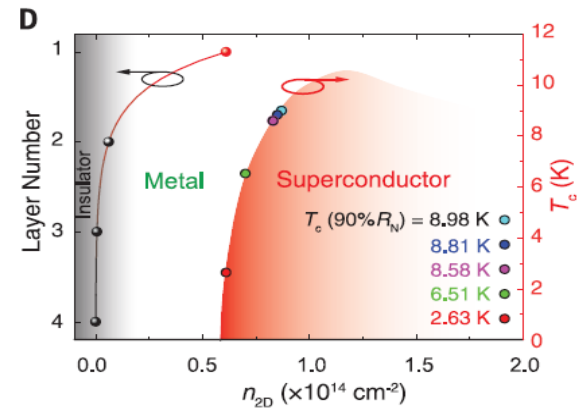
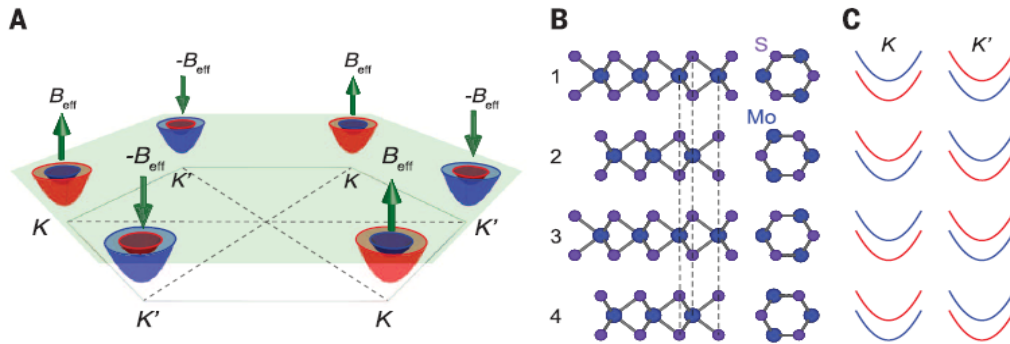
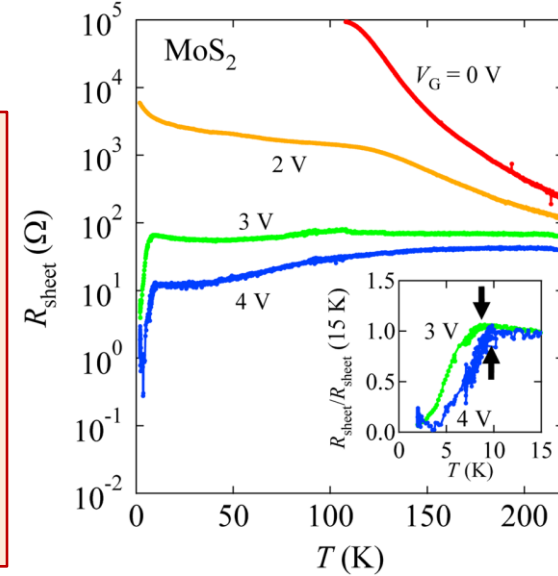


Fig. 1. Inducing superconductivity in thin flakes of MoS_2 by gating. (A) Conduction-band electron pockets near the K and K' points in the hexagonal Brillouin zone of monolayer MoS_2 . Electrons in opposite K and K' points experience opposite effective magnetic fields \mathbf{B}_{eff} and $-\mathbf{B}_{\text{eff}}$, respectively (green arrows). The blue and red colored pockets indicate electron spins oriented up and down, respectively. (B) Side view (left) and top view (right) of the four outermost layers in a multilayered MoS_2 flake. The vertical dashed lines show the relative positions of Mo and S atoms in $2H$ -type stacking. In-plane inversion symmetry is broken in each individual layer, but global inversion symmetry is restored in bulk after stacking. (C) Energy-band splitting caused by \mathbf{B}_{eff} . Blue and red bands denote spins aligned up and down, respectively. Because of $2H$ -type stacking, adjacent layers have opposite \mathbf{B}_{eff} at the same K points. (D) The red curve (left axis) denotes the theoretical carrier density n_{2D} for the four outermost layers of MoS_2 (26) for sample D1, when $T_C(0) = 2.37\text{ K}$. In the phase diagram (right axis), superconducting states with different values of $T_C(0)$ are color-coded; the same color-coding is used across all figures. Here, T_C is determined at the temperature where the resistance drop reaches 90% of R_N at 15 K. This criterion is different from the 50% R_N criterion used in the rest of the paper; it was chosen to be consistent with that used in the phase diagram of (17). (E) Temperature dependence of R_s , showing different values of T_C corresponding to superconducting states (from samples D1 and D24) denoted in (D).

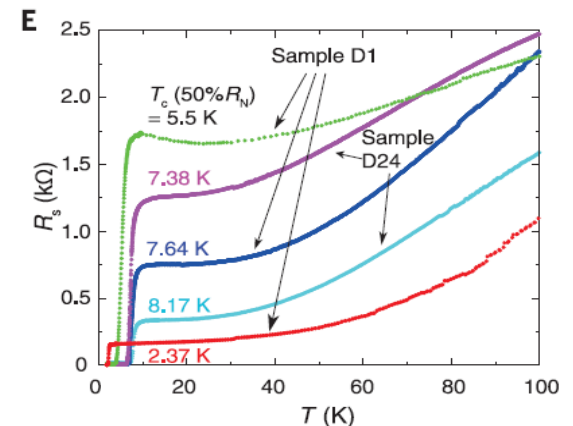
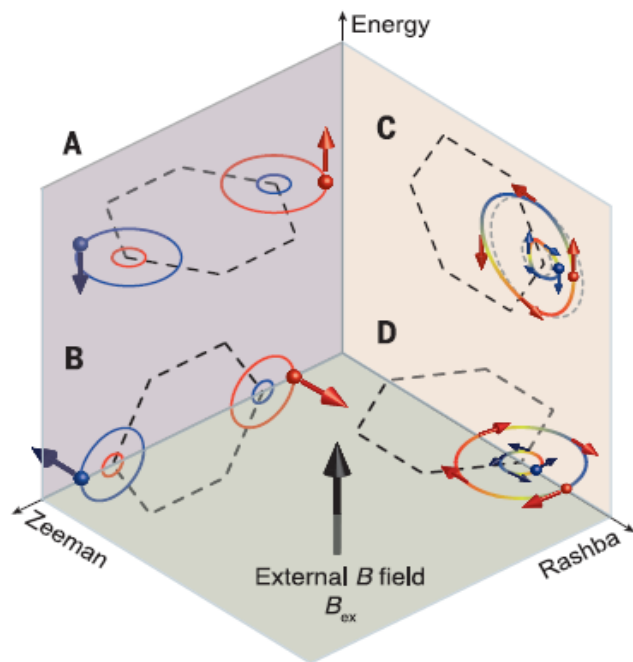
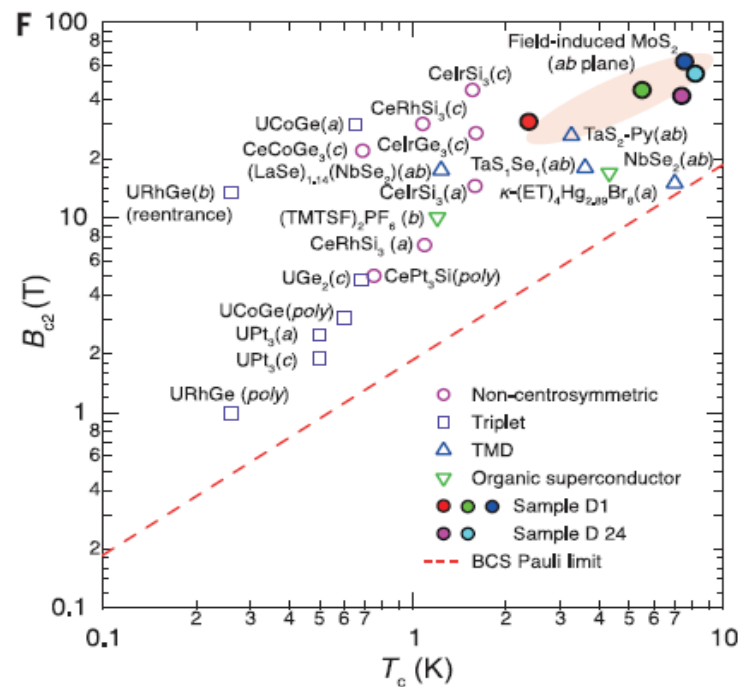
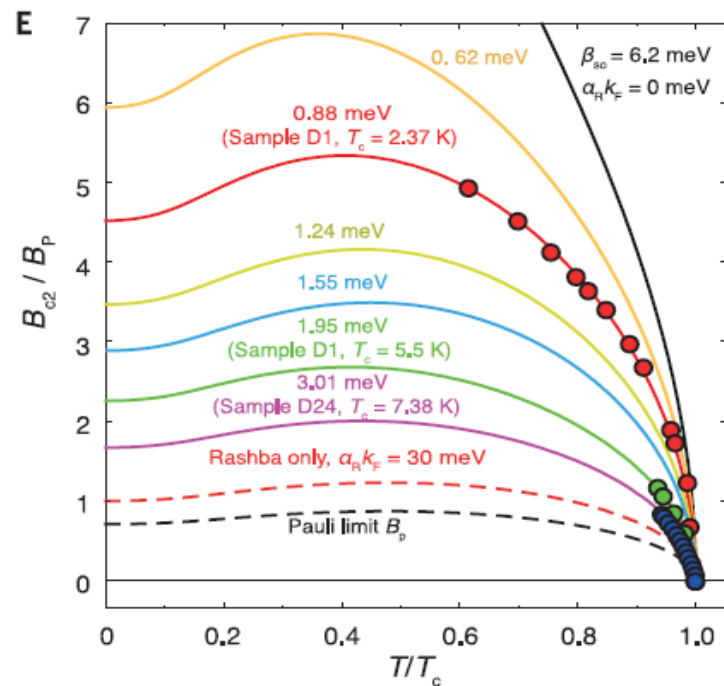


Fig. 4. Interplay between an external magnetic field and the spins of Cooper pairs aligned by Zeeman and Rashba-type effective magnetic fields. (A to D)

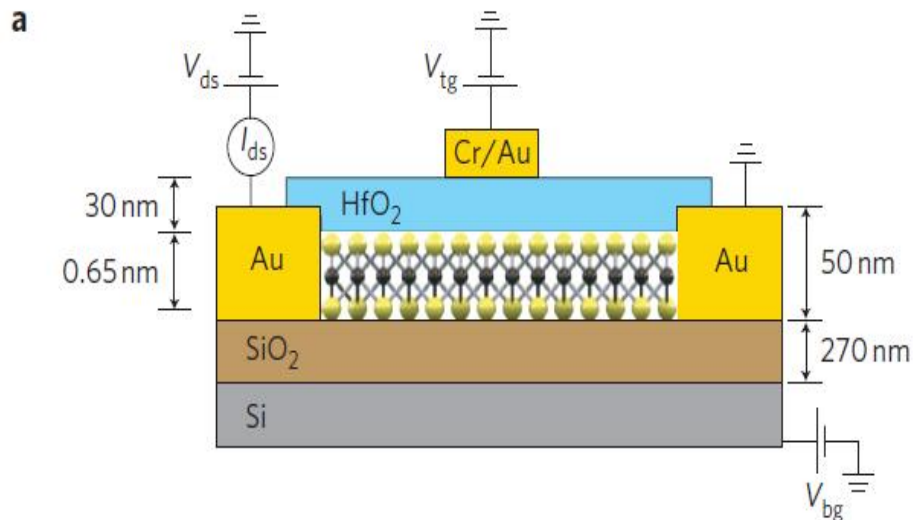
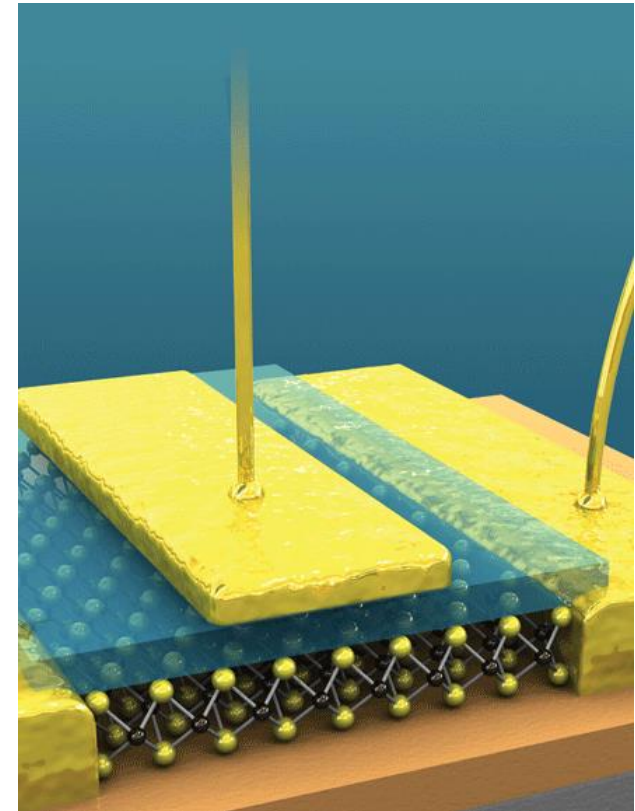


When Rashba or Zeeman SOC aligns the spins of Cooper pairs parallel to the external field, the increase in Zeeman energy due to parallel coupling between the field and the spin eventually can cause the pair to break [(A) and (C)]. In (B) and (D), the acquired Zeeman energy is minimized as a result of the orthogonal coupling between the field and the aligned spins, which effectively protects the Cooper pairs from depairing. (E) Theoretical fitting of the relationship between B_{c2}/B_p and T/T_c for samples D1 [$T_c(0) = 2.37$ K and 5.5 K] and D24 [$T_c(0) = 7.38$ K], using a fixed effective Zeeman field ($\beta_{SD} = 6.2$ meV) and an increasing Rashba field ($\alpha_R k_F$ ranges from 10 to $\sim 50\%$ of β_{SD}) [section 6 of (16)]. Two dashed lines show the special cases calculated by equation S3, when only the Rashba field ($\alpha_R k_F = 30$ meV; $\beta_{SD} = 0$) is considered (red), and when both the Zeeman and Rashba fields are zero (black). In the former case, a large $\alpha_R k_F$ causes a moderate increase of B_{c2} to $\sim \sqrt{2} B_p$ (10). In the latter case, the conventional Pauli limit at zero temperature is recovered. (F) Plot of B_{c2} versus T_c for different superconductors [a magnetic field was applied along crystal axes a , b , or c or to a polycrystalline ($poly$)]. The data shown are from well-known systems including noncentrosymmetric (pink circles), triplet (purple squares) (6, 8, 9), low-dimensional organic (green triangles) (40, 50–52), and bulk TMD superconductors (blue triangles) (35–38, 47). The robustness of the spin protection can be measured by the vertical distance between B_{c2} and the red dashed line denoting B_p . Gate-induced superconductivity from samples D1 and D24 are among the states with the highest B_{c2}/B_p ratio. In $(\text{LaSe})_{1-4}(\text{NbSe}_2)_x$, T_c was determined at 95% of R_N ; T_c in organic molecule–intercalated TMDs was obtained by extrapolating to zero resistance; and all other systems use the standard of 50% of R_N .



Field-effect transistors (FETs) based on MoS₂.

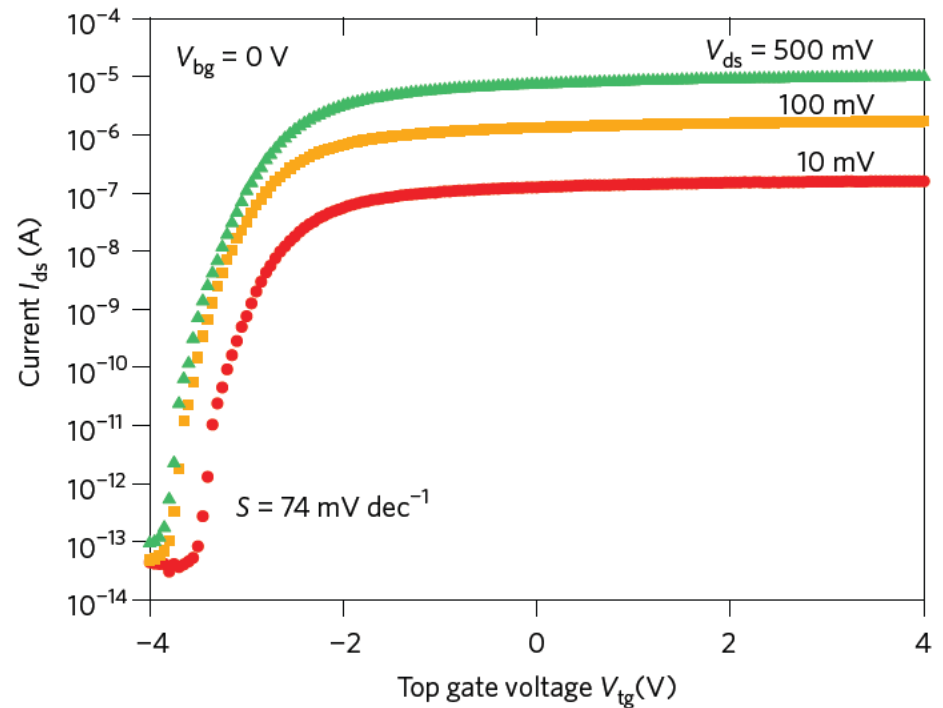
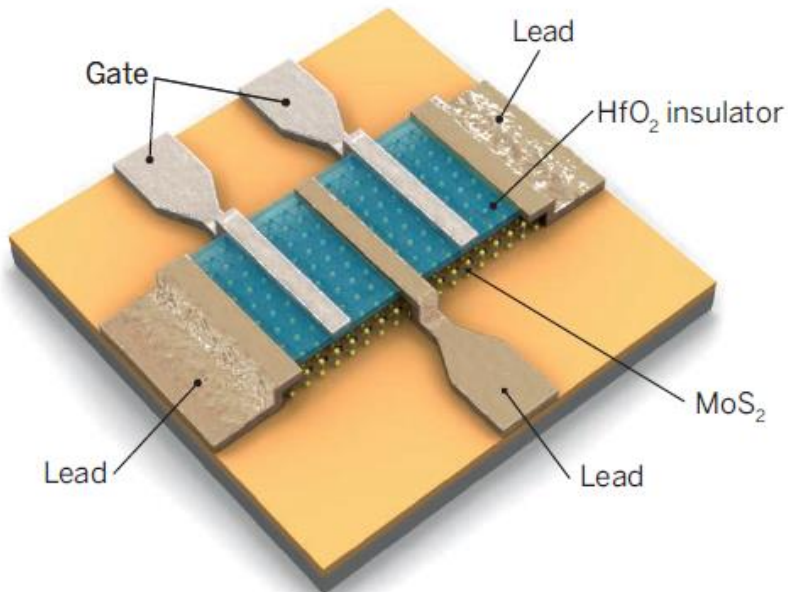
Andras Kis and co-workers have made an FET in which the channel is a single layer of MoS₂ that is just 0.65 nm thick and 1,500 nm long: the black spheres in this schematic are Mo atoms; the yellow spheres are S atoms. The MoS₂ layer also has a bandgap, which is crucial for many applications.



Andras Kis et al, Nature Nanotech.
6, No 3, 146, (2011).

MoS₂

- ❑ Switch on and off at 10⁹ times/sec, a large on/off ratio, making it easy to differentiate between digital 1s and 0s.
- ❑ A Mobility ~ 200; and was later corrected to ~15.



Researchers have made quick progress in turning 2D materials into devices, such as this simple circuit in which two transistors use MoS₂ to ferry charges between electrode leads.

Andras Kis, Nature Nanotechnology
Vol 6, No 3, 146, (2011).

Field-Effect Mobility (review)

Monolayer MoS₂

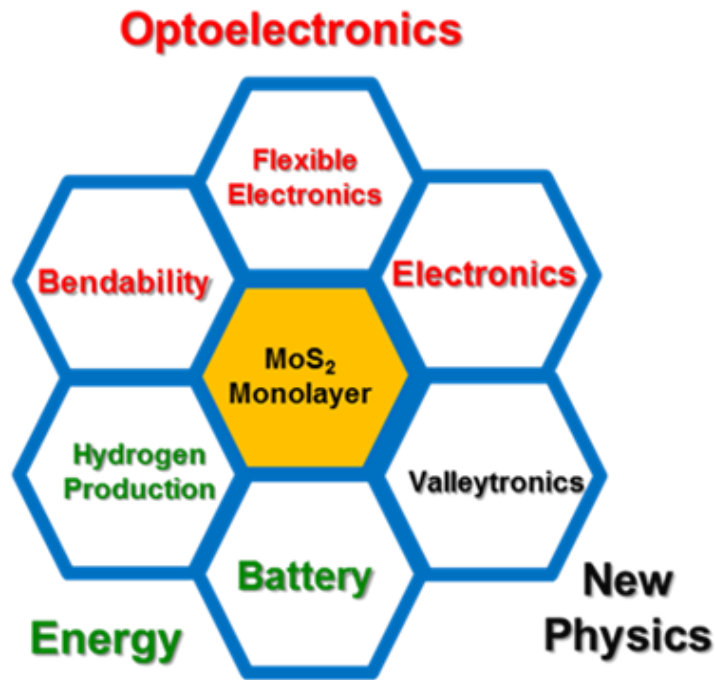
- Room temperature mobility
- Back-gated Silicon oxide : **0.1 - 50** cm²/V.s SS:
1cm²/V.s
- Dual gate (SiO₂+HfO₂): **15** cm²/V sec
- Original ~200: Nat Nanotechnol **6**, 147 (2011)
- Correction ~ 15: Nat Nanotechnol **8**, 147 (2013)
- On/off ratio: 10⁸

Multilayer MoS₂

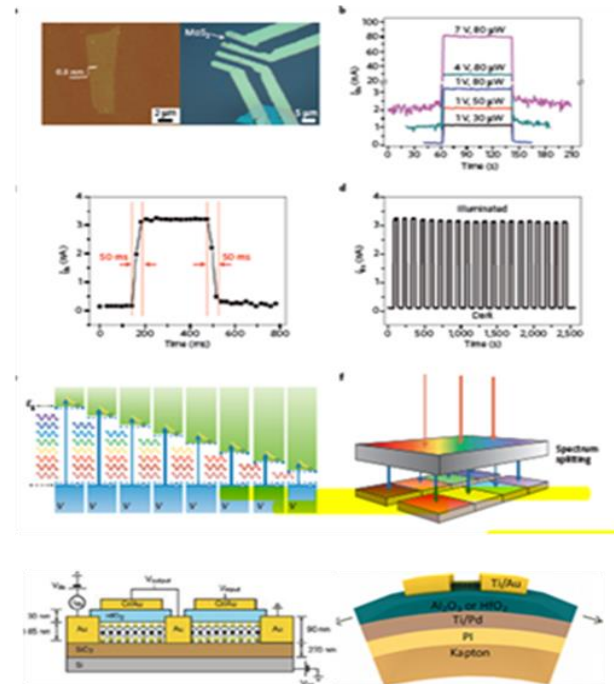
- Back-gated Al₂O₃: **100** cm²/Vsec
- multilayer MoS₂: 30nm
- On/off ratio: 10⁶
Nature Communications, 3, 1011 (2012)
- On PMMA: 470cm²/V.s(electrons)
480cm²/V.s(holes)
APL 102(4), 042104 (2013)

MoS₂ Optoelectronics

- MoS₂'s strong interactions with light would be favorable for solar cells, light emitters, and other optical devices.



Flexible optoelectronics



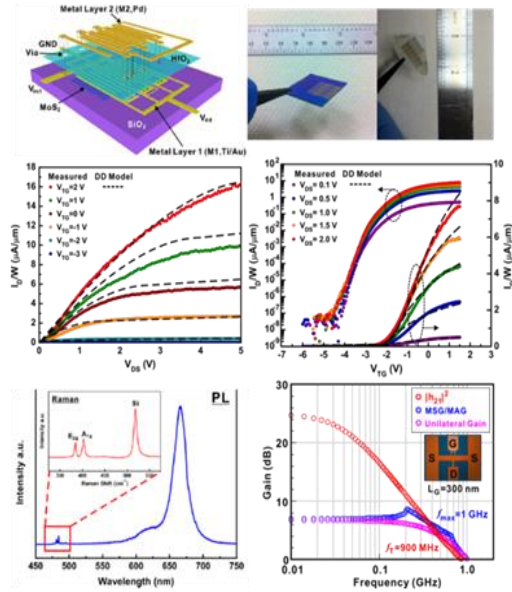
QH Wang et al,
Nat. Nano, 7, p699 (2012)

Applications: Electronics

Large-scale CVD-MoS₂ Monolayer Devices:

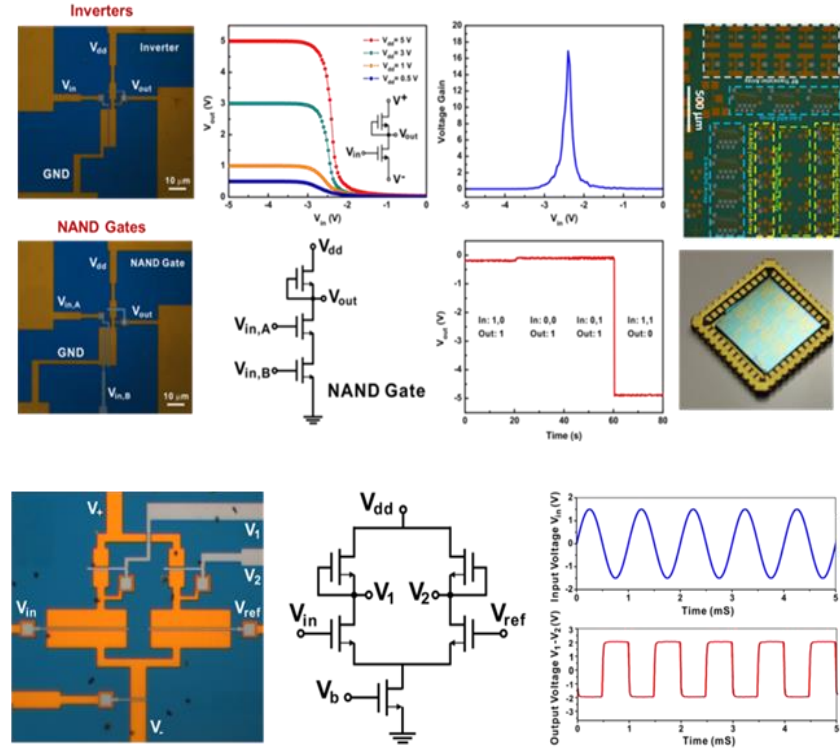
H. Wang, L. Yu, YH Lee et. al., *IEDM Tech. Digest*, 2012

-the best paper award in IEDM 2012



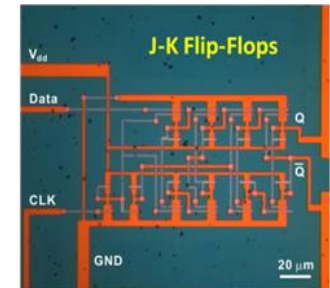
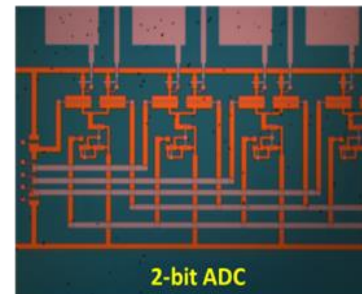
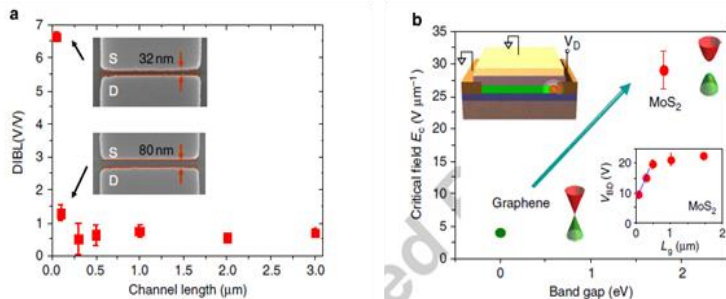
CVD-MoS₂ Monolayer Mixed-signal Circuits

H. Wang, YH Lee et. al., (in-preparation)

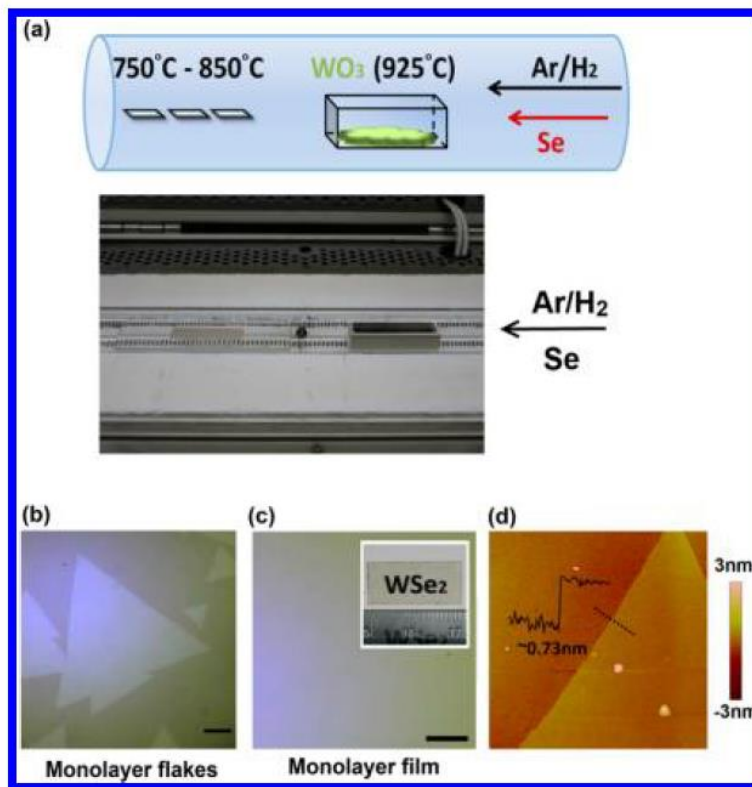


Electronic transport of CVD-MoS₂ Monolayer

W. Zhu, and YH Lee et. al., *Nat. Comm.* 5,3087 (2014)

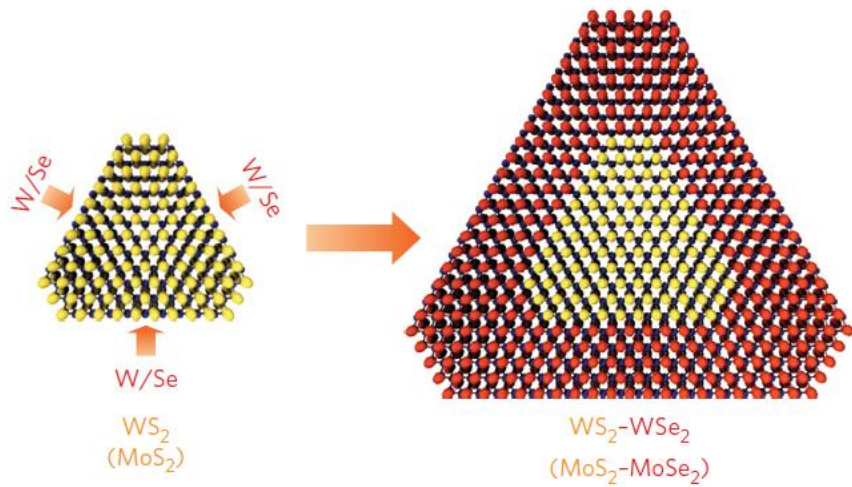


MoS₂ and WS₂ CVD growth



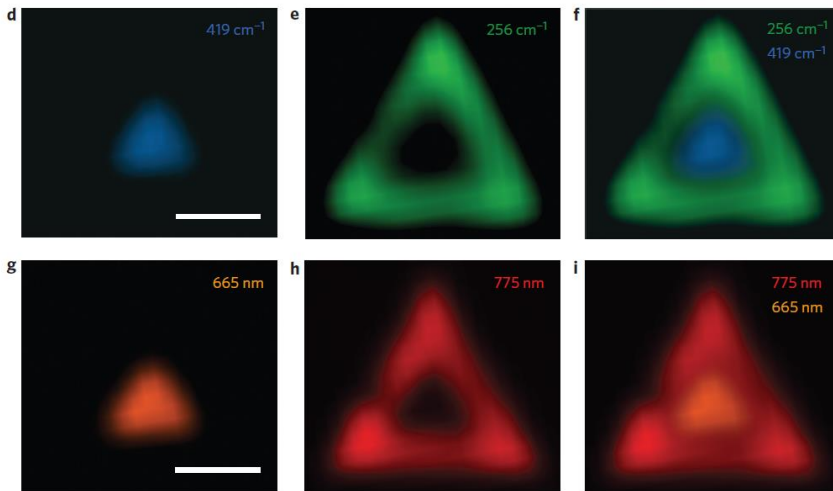
- (a) Schematic illustration for the growth of WSe₂ layers on sapphire substrates by the reaction of WO₃ and Se powders in a CVD furnace. A photo of the setup is also shown.
- (b) and (c) Optical microscopy images of the WSe₂ monolayer flakes and monolayer film grown at 850 and 750 C, respectively. Scale bar is 10 μm in length. The inset in (c) shows the photograph of a uniform monolayer film grown on a double side polished sapphire substrate.
- (d) AFM image of a WSe₂ monolayer flake grown at 850 C on a sapphire substrate.

MoS₂ and WS₂ Lateral Epitaxy



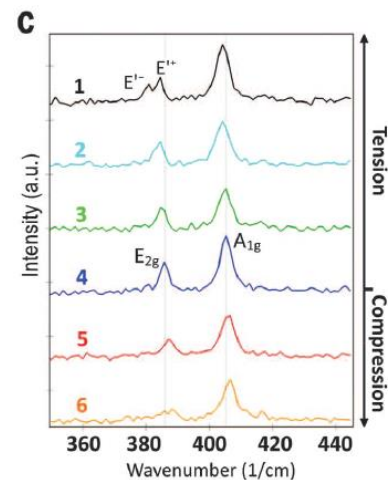
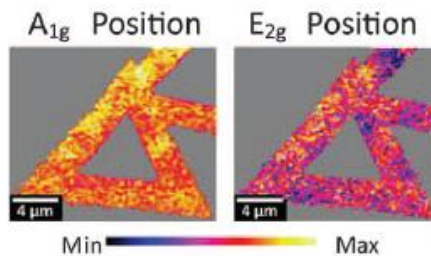
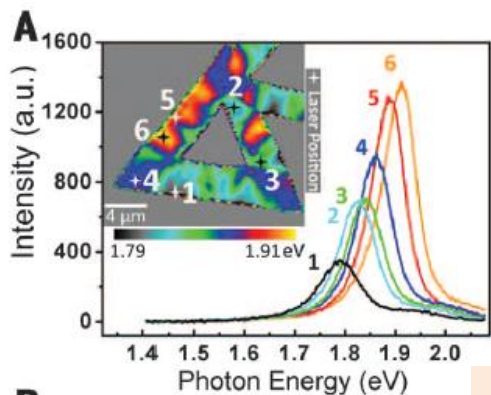
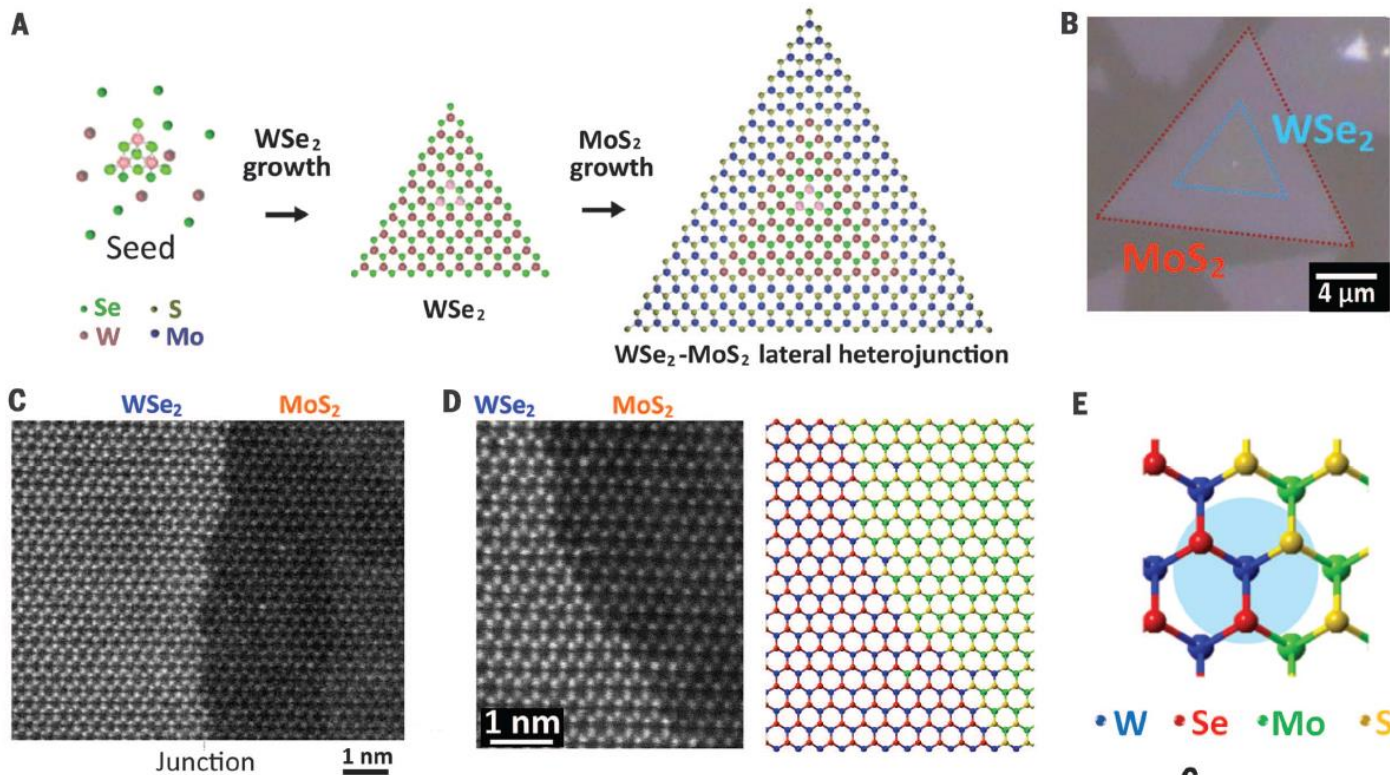
Schematic of lateral epitaxial growth of WS₂-WSe₂ and MoS₂-MoSe₂ heterostructures.

- A triangular domain of WS₂ (MoS₂) is first grown using a CVD process.
- The peripheral edges of the triangular domain feature unsaturated dangling bonds that function as the active growth front for the continued addition, and incorporation of precursor atoms to extend the two dimensional crystal in the lateral direction.



d, Raman mapping at 419 cm⁻¹ (WS₂ A1g signal), demonstrating that WS₂ is localized at the center region of the triangular domain. e, Raman mapping at 256 cm⁻¹ (WSe₂ A1g signal), demonstrating that WSe₂ is located in the peripheral region of the triangular domain. f, Composite image consisting of Raman mapping at 256 cm⁻¹ and 419 cm⁻¹, showing no apparent overlap or gap between the WS₂ and WSe₂ signals, demonstrating that the WS₂ inner triangle and WSe₂ peripheral areas are laterally connected. g, h, photoluminescence mapping images at 665 nm and 775 nm, showing characteristic photoluminescence emission of WS₂ and WSe₂ in the center and peripheral regions of the triangular domain, respectively. i, Composite image consisting of photoluminescence mapping at 665 nm and 775 nm, demonstrating the formation of WS₂-WSe₂ lateral heterostructures.

WSe₂-MoS₂ lateral p-n junction with an atomically sharp interface



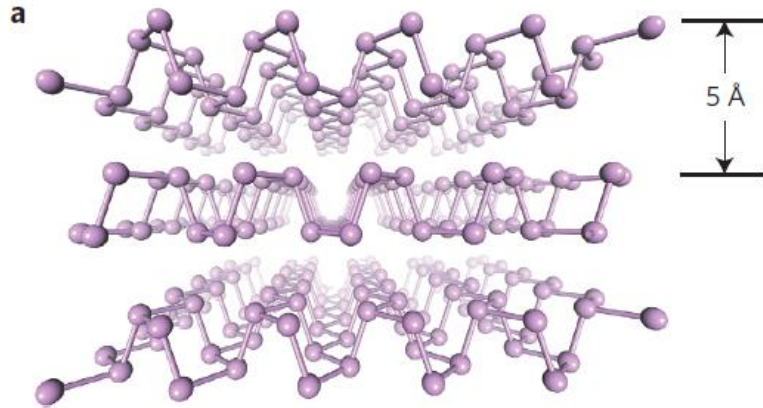
W. H. Chang, Science, 349, 524, (2015)

Graphene-like Series

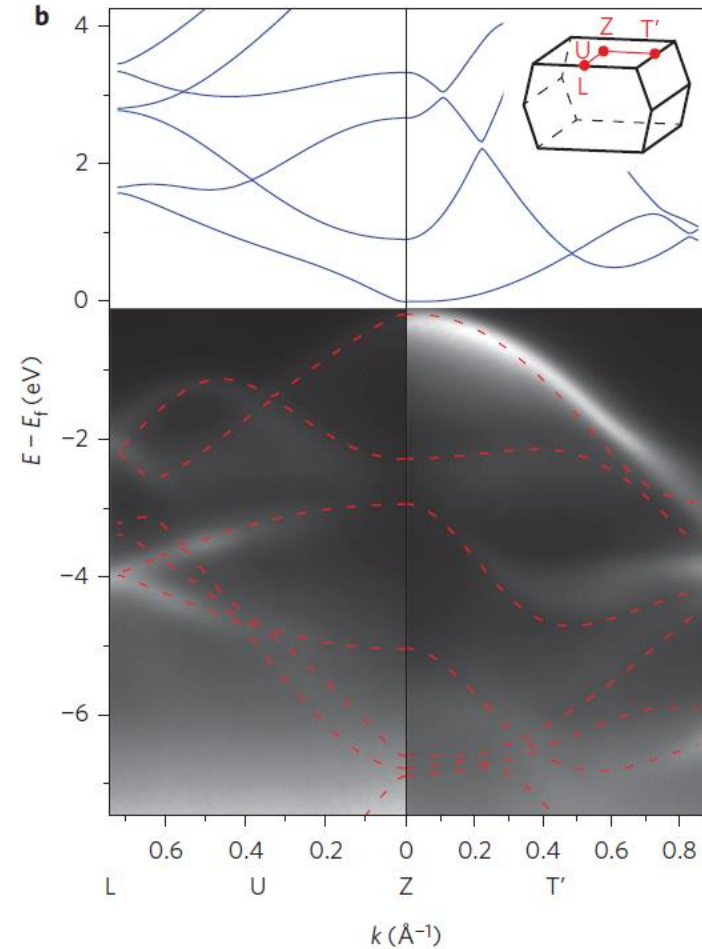
Phosphorene

- **Black phosphorus**, phosphorene is one of three different crystal structures that pure phosphorus can adopt.
- White phosphorus is used in making fireworks.
- Red phosphorus is used to make the heads of matches.
- The bandgap is adjusted by varying the number of phosphorene layers stacking one atop another, significantly larger than the bulk value of 0.31- 0.36 eV.
- Much easier to engineer devices with the exact behavior desired.
- **Mobility ~ 600**
- Unstable in air.
- Passivated by Al_2O_3 layer and teflon.
- Harnessing phosphorene's higher electron mobility for making electronic devices.

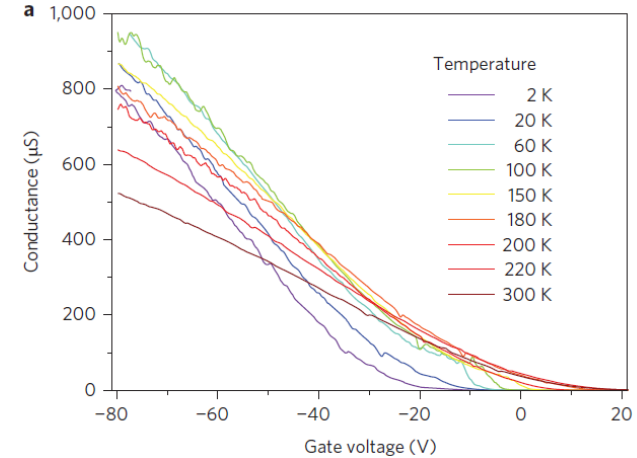
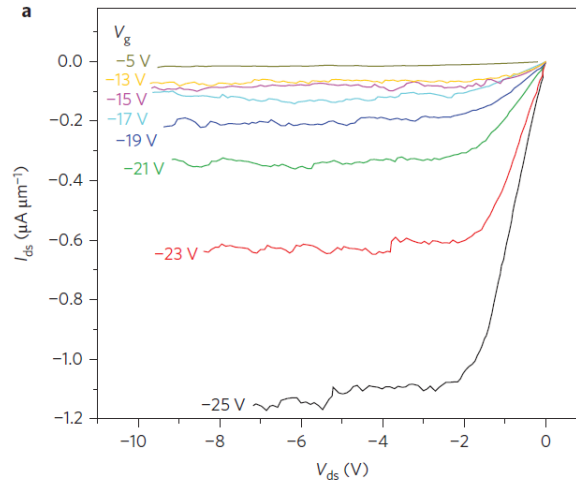
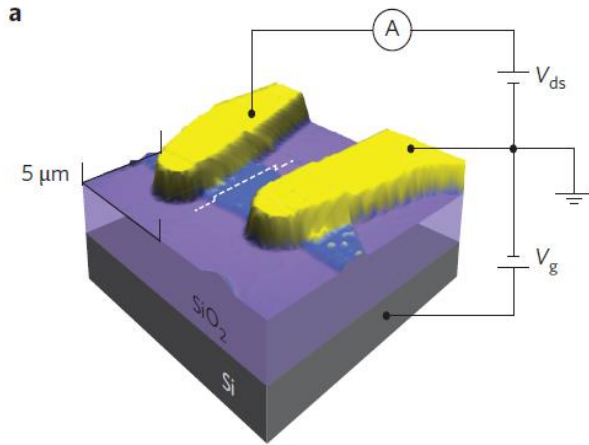
Phosphorene



- Black phosphorus was synthesized under a constant pressure of 10 kbar by heating red phosphorus to 1,000 C .
- Then slowly cooling to 600 C at a cooling rate of 100 C per hour.



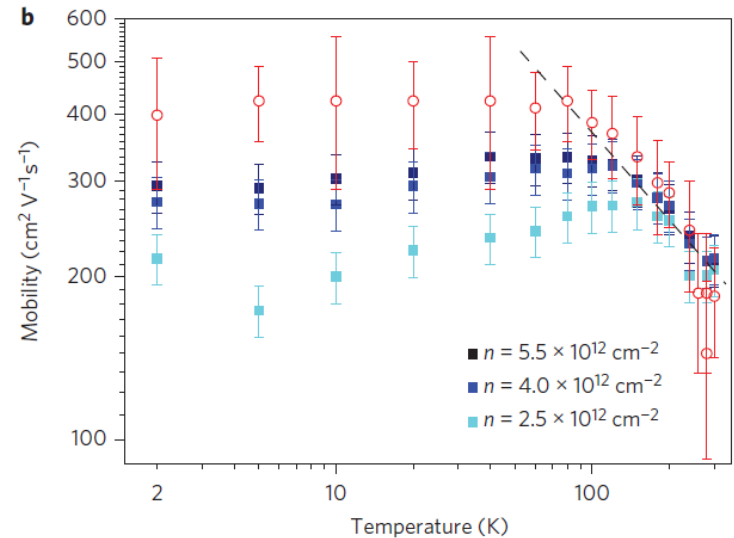
Phosphorene



- ❑ Reliable transistor performance is achieved at room temperature in samples thinner than 7.5 nm. Channel length and width of the device are 1.6 mm and 4.8mm.
- ❑ Field-effect mobility (red open circles), and Hall mobility (filled squares, three different values of n) as a function of temperature on a logarithmic scale

❑

$$\mu_{FE} = \frac{L}{W} \frac{1}{C_g} \frac{dG}{d(V_g - V_{th})} \quad \mu_H = \frac{L}{W} \frac{G}{ne}$$



Phosphorene

- fabricating p-type FETs based on few-layer phosphorene.
- exhibit ambipolar behavior with drain current modulation up to 10^5 ,
- a field-effect mobility to $1,000 \text{ cm}^2 \text{ V}^{-1} \text{ s}^{-1}$ at room temperature, and thickness dependent.

Tomanek at Michigan State, and Peter Ye at Purdue reported phosphorene-based transistors, along with simple circuits. ACS Nano, 8 (4), pp 4033–4041, (2014).

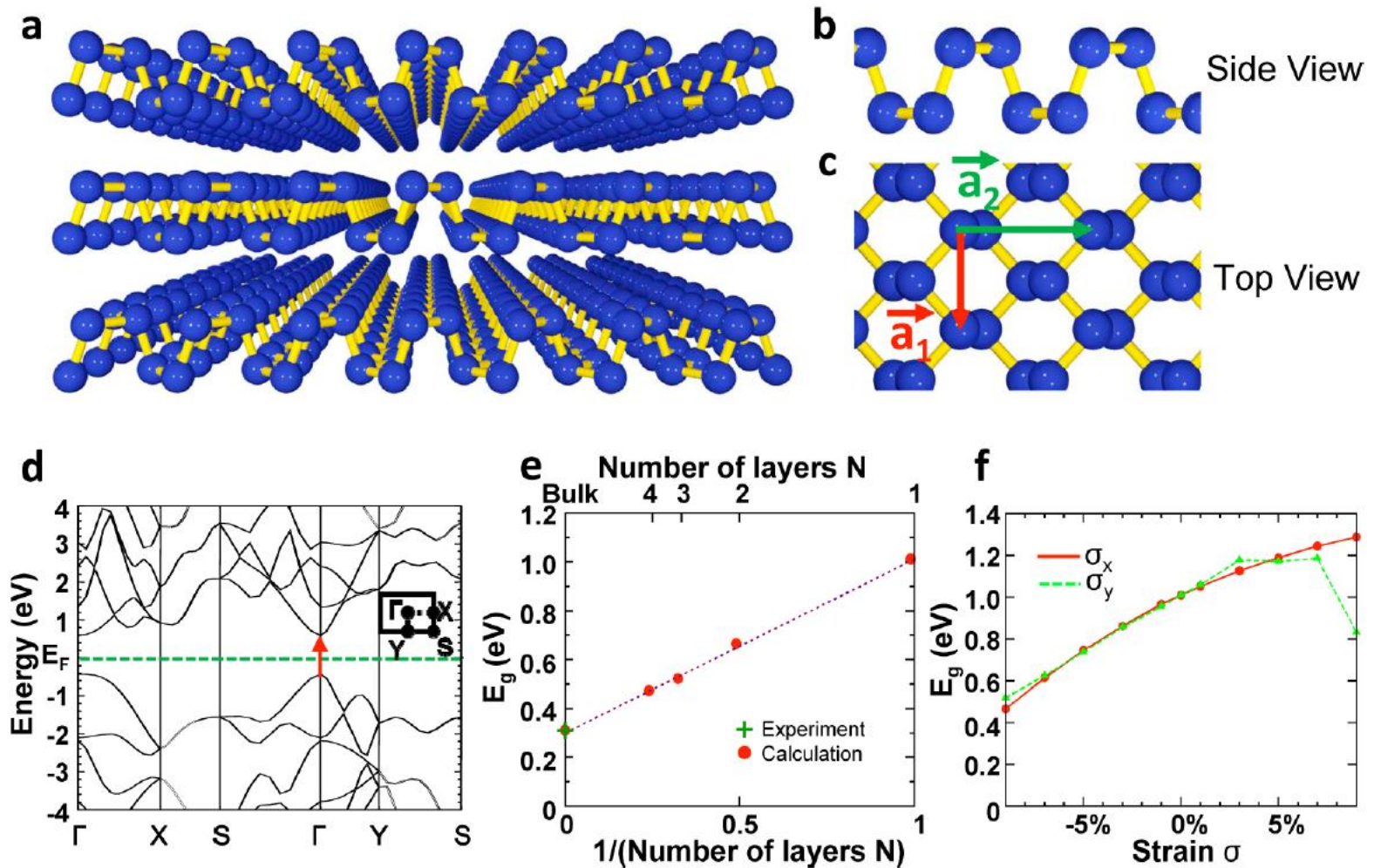
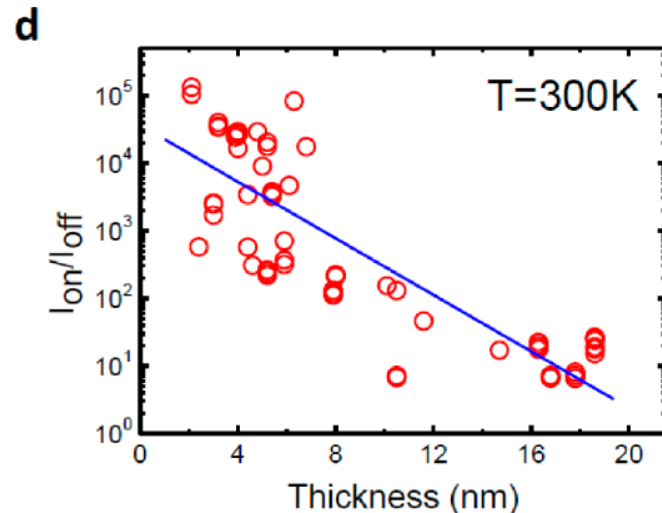
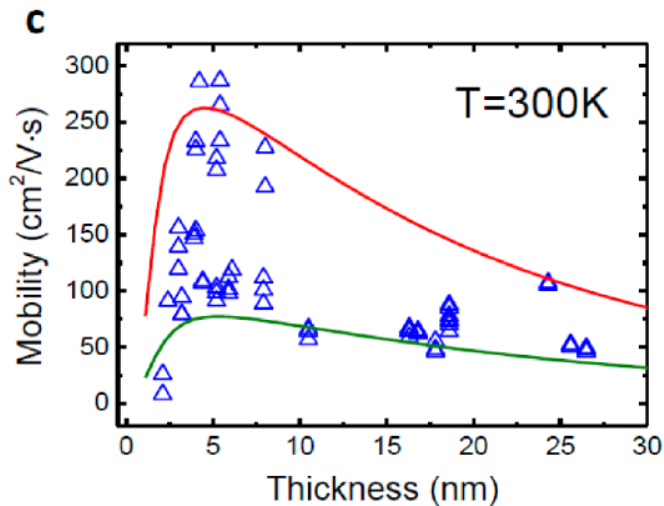
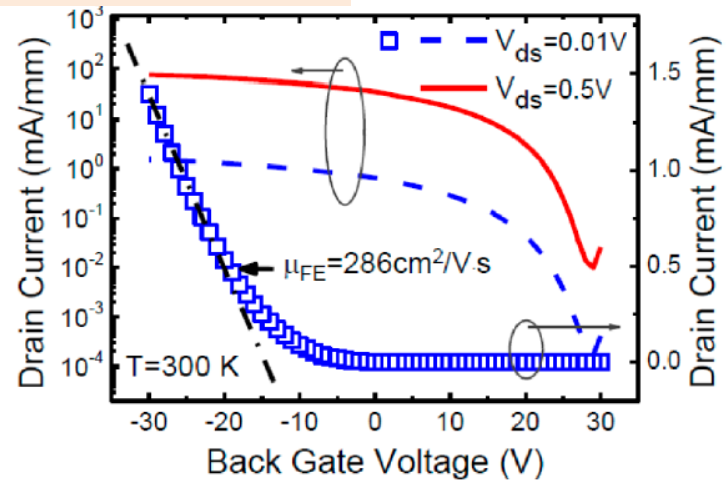
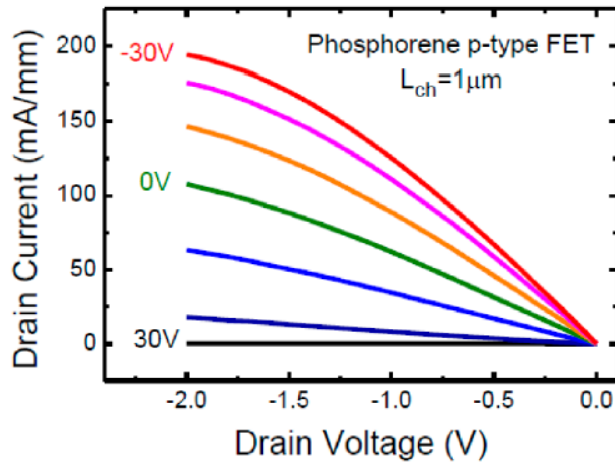


Figure 1. Crystal structure and band structure of few-layer phosphorene. (a) Perspective side view of few-layer phosphorene. (b,c) Side and top views of few-layer phosphorene. (d) DFT-HSE06 band structure of a phosphorene monolayer. (e,f) DFT-HSE06 results for the dependence of the energy gap in few-layer phosphorene on (e) the number of layers and (f) the strain along the x- and y-direction within a monolayer. The observed band gap value in the bulk is marked by a cross in (e).

Phosphorene-based field effect transistors

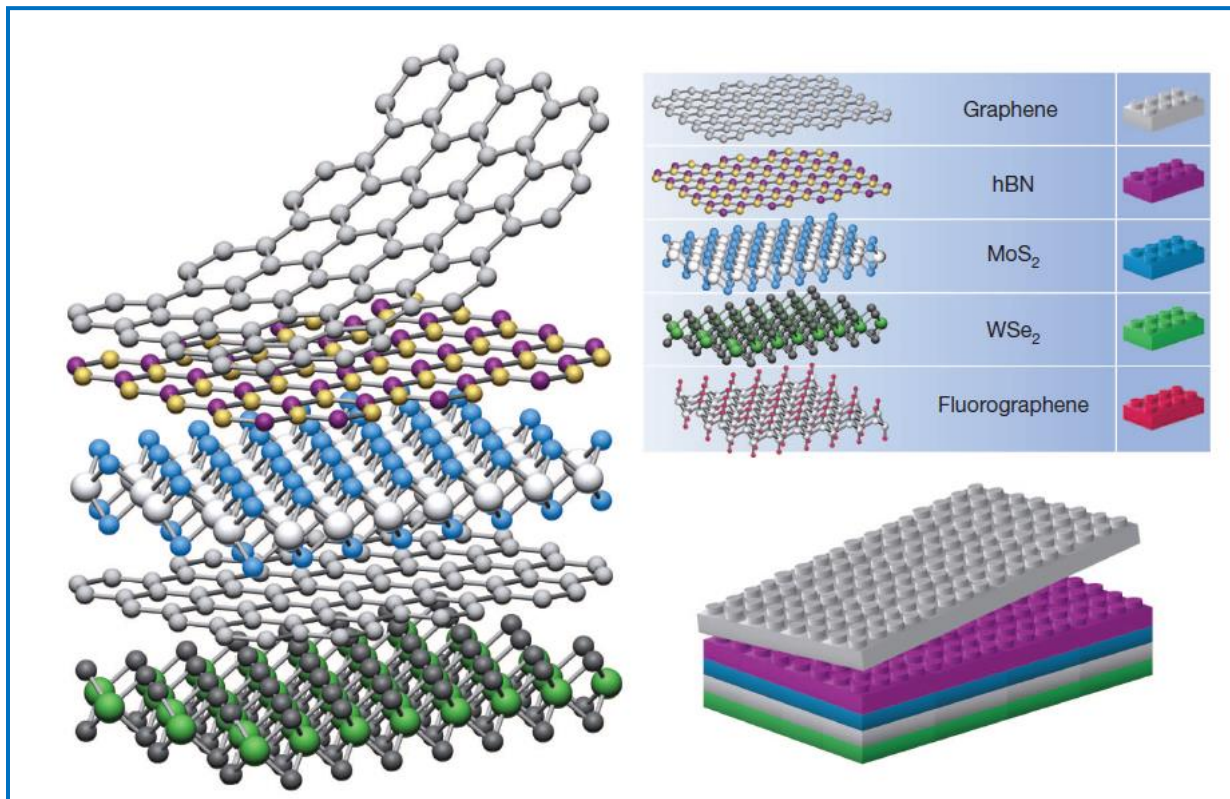


- Tomanek and Ye reported to have made phosphorene-based transistors, along with simple circuits. [ACS Nano, 8 \(4\), p. 4033–4041, \(2014\).](#)
- A few-layer phosphorene FET with $1.0 \mu\text{m}$ channel length displays a high on-current of 194 mA/mm, a high hole field-effect mobility of $286 \text{ cm}^2/\text{V}\cdot\text{s}$, and an on/off ratio of up to 10^4 .
- Constructed a **CMOS inverter** by a phosphorene PMOS transistor and a MoS_2 NMOS transistor.

2-D Hetero-structures and applications

- ❑ Two-dimensional materials offer stacked like cards in a deck to create the different electronic layers as needed in functional electronic devices.
- ❑ Because they do not form tight bonds with the layers above and below.
- ❑ Ye's group at Purdue reported to use both MoS₂ and phosphorene to make ultrathin photovoltaics (PVs).
- ❑ Geim et al reported in Nature Materials to have assembled multiple 2D materials to make efficient thin LEDs.
- ❑ Revolution in electronics and optics just began.
- ❑ Flexible, transparent, temperature stable, and cheap to manufacture

Van der Waals heterostructures



Building van der Waals Heterostructures:

If one considers 2D crystals to be analogous to Lego blocks (right panel), the construction of a huge variety of layered structures becomes possible.

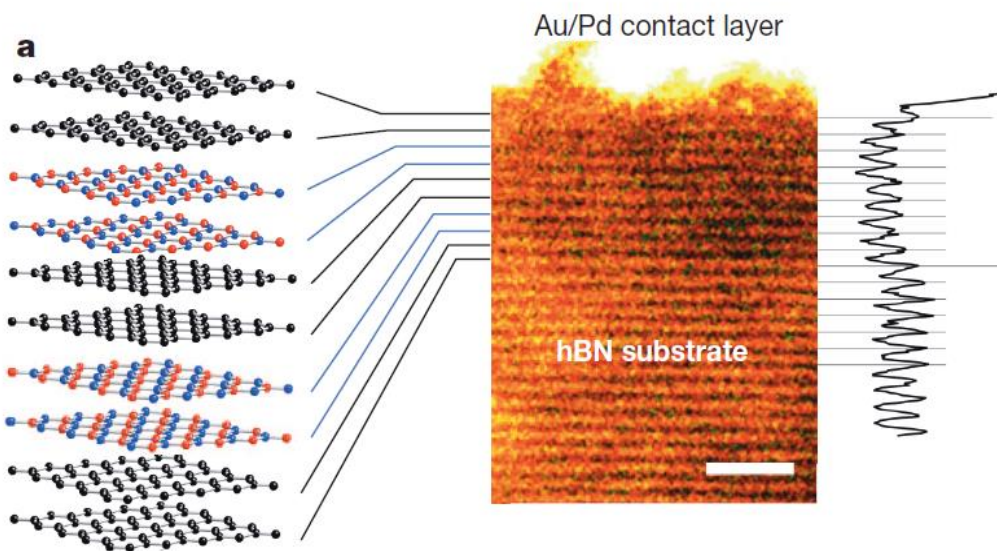
Conceptually, this atomic scale Lego resembles molecular beam epitaxy but employs different 'construction' rules and a distinct set of materials.

Current 2D library

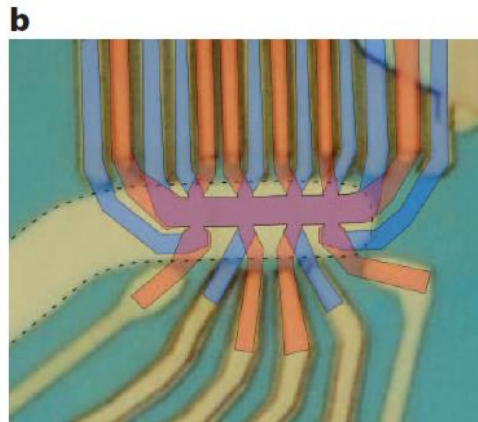
Monolayers proved to be stable under ambient conditions (room temperature in air) are shaded **blue**; those probably stable in air are shaded **green**; and those unstable in air but that may be stable in inert atmosphere are shaded **pink**. **Grey** shading indicates 3D compounds that have been successfully exfoliated down to monolayers, as is clear from atomic force microscopy, for example, but for which there is little further information. We note that, after intercalation and exfoliation, the oxides and hydroxides may exhibit stoichiometry different from their 3D parents (for example, TiO_2 exfoliates into a stoichiometric monolayer of $\text{Ti}_{0.87}\text{O}_2$).

Graphene family	Graphene	hBN 'white graphene'	BCN	Fluorographene	Graphene oxide
2D chalcogenides	MoS ₂ , WS ₂ , MoSe ₂ , WSe ₂	Semiconducting dichalcogenides: MoTe ₂ , WTe ₂ , ZrS ₂ , ZrSe ₂ and so on		Metallic dichalcogenides: NbSe ₂ , NbS ₂ , TaS ₂ , TIS ₂ , NiSe ₂ and so on	
				Layered semiconductors: GaSe, GaTe, InSe, Bi ₂ Se ₃ and so on	
2D oxides	Micas, BSCCO	MoO ₃ , WO ₃	Perovskite-type: LaNb ₂ O ₇ , (Ca,Sr) ₂ Nb ₃ O ₁₀ , Bi ₄ Ti ₃ O ₁₂ , Ca ₂ Ta ₂ TiO ₁₀ and so on		Hydroxides: Ni(OH) ₂ , Eu(OH) ₂ and so on
	Layered Cu oxides	TiO ₂ , MnO ₂ , V ₂ O ₅ , TaO ₃ , RuO ₂ and so on			Others

State-of-the-art van der Waals structures and devices

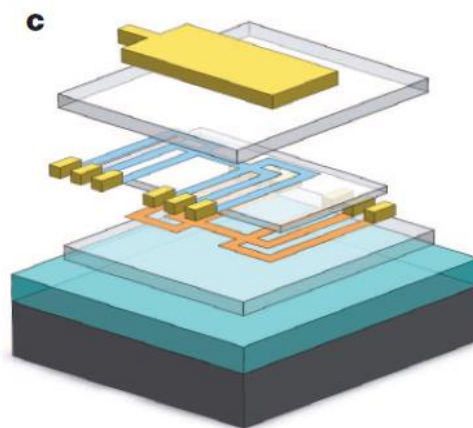


a, Graphene-hBN superlattice consisting of six stacked bilayers. On the right its cross-section and intensity profile as seen by scanning transmission electron microscopy are shown; on the left is a schematic view of the layer sequence. The topmost **hBN** bilayer is not visible, being merged with the metallic contact.

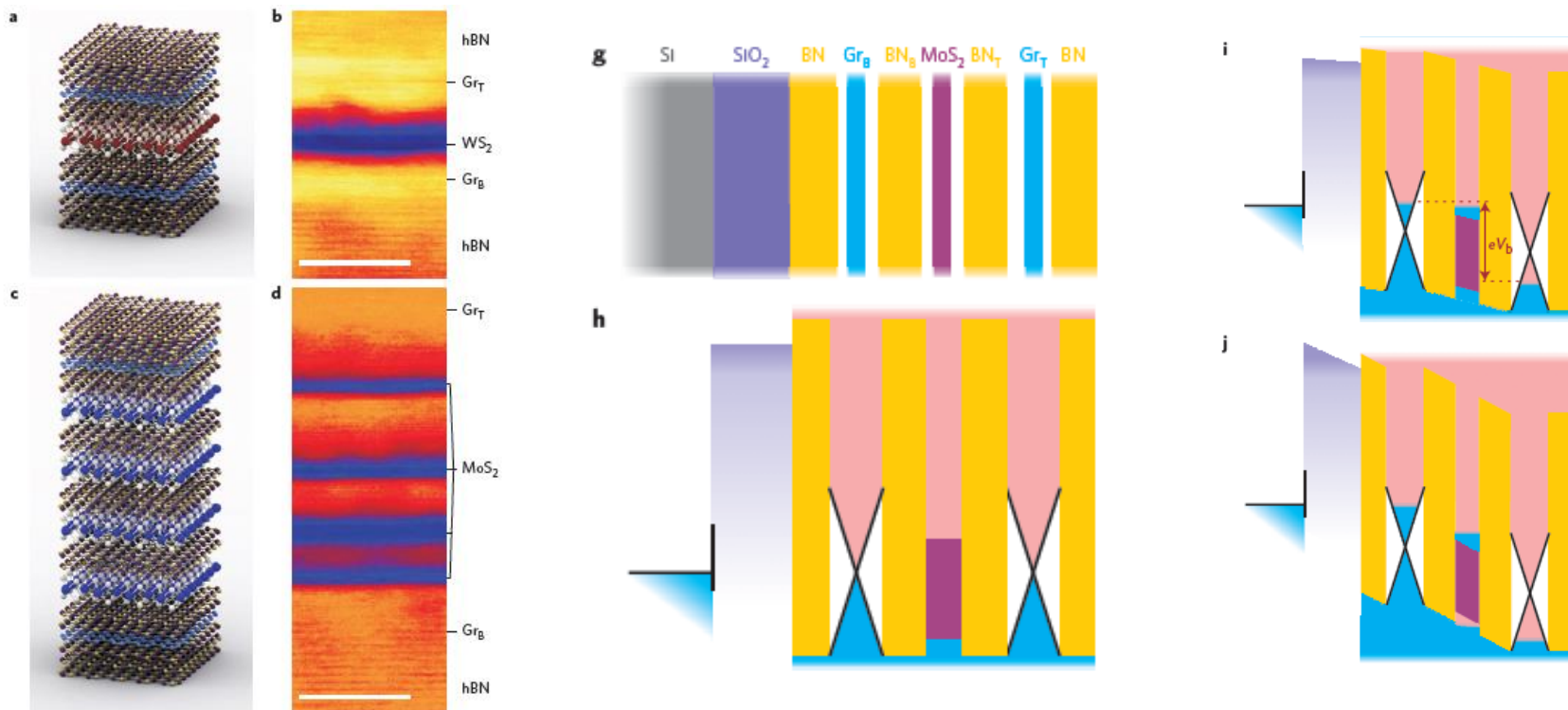


b, c, Double-layer graphene

heterostructures. An optical image of a working device (b), and its schematics in matching colors (c). Two graphene Hall bars are accurately aligned, separated by a trilayer hBN crystal and encapsulated between relatively thick hBN crystals (hBN is shown in c as semitransparent slabs). The entire heterostructure is placed on top of an oxidized Si wafer (SiO₂ is in turquoise). The colors in b indicate the top (blue) and bottom (orange) Hall bars and their overlapping region (violet). The graphene areas are invisible in the final device image because of the top Au gate outlined by dashes. The scale is given by the width of the Hall bars, 1.5 μm.



Heterostructure devices with SQW and MQWs by band structure engineering



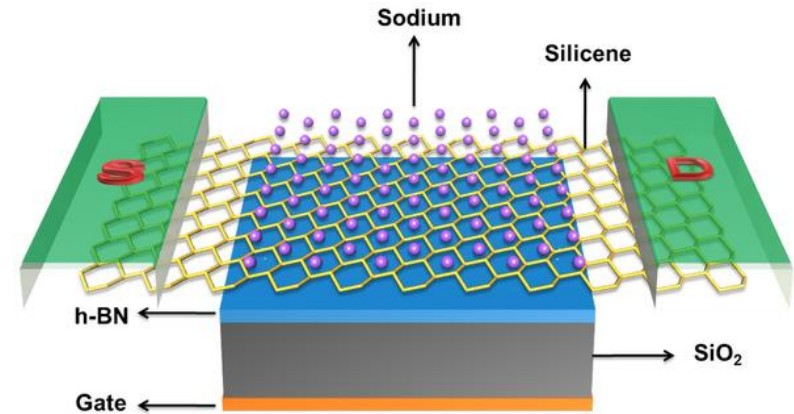
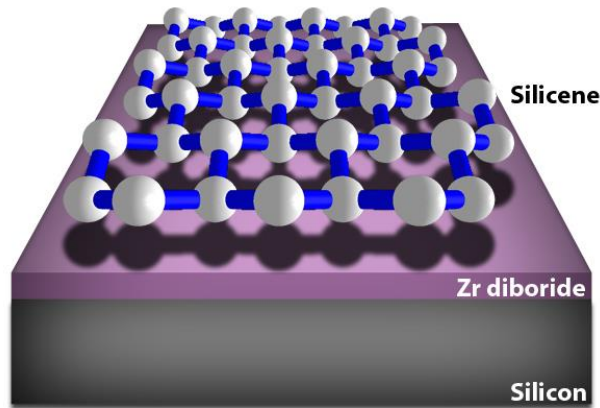
- a**, Schematic of the SQW heterostructure : $\text{hBN}/\text{Gr}_B/2\text{hBN}/\text{WS}_2/2\text{hBN}/\text{Gr}_T/\text{hBN}$.
- b**, Cross-sectional bright-field STEM image of the type of heterostructure presented in **a**. Scale bar, 5 nm.
- c,d**, Schematic and STEM image of the MQW heterostructure : $\text{hBN}/\text{Gr}_B/2\text{hBN}/\text{MoS}_2/2\text{hBN}/\text{MoS}_2/2\text{hBN}/\text{MoS}_2/2\text{hBN}/\text{MoS}_2/2\text{hBN}/\text{Gr}_T/\text{hBN}$. The number of hBN layers between MoS₂ QWs in **d** varies. Scale bar, 5 nm.
- g**, Schematic of the heterostructure $\text{Si}/\text{SiO}_2/\text{hBN}/\text{Gr}_B/3\text{hBN}/\text{MoS}_2/3\text{hBN}/\text{Gr}_T/\text{hBN}$.
- h–j**, Band diagrams for the case of zero applied bias (**h**); intermediate applied bias (**i**); and high bias (**j**) for the heterostructure presented in **g**.

Silicene, Germanene, and Stanene

- To investigate the growth and characterizations for novel graphene-derived 2D materials such as *silicene, germanene, and stanene*.
- Stanene is recently predicted to be quantum spin Hall (QSH) insulator with a large bulk gap ~ 0.3 eV.
- Their QSH states can be effectively tuned by chemical functionalization and external strain, viable for low-power-consumption electronics.

Another emerging wonder material : Silicene

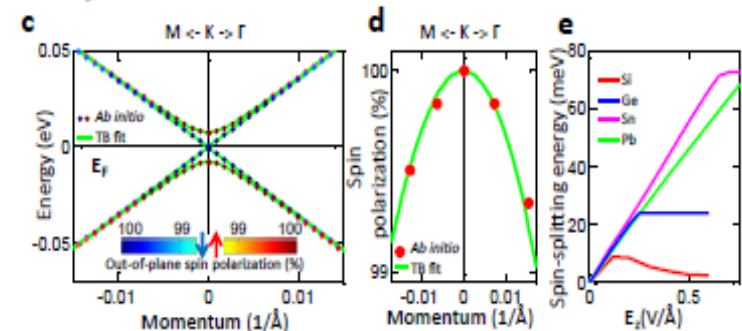
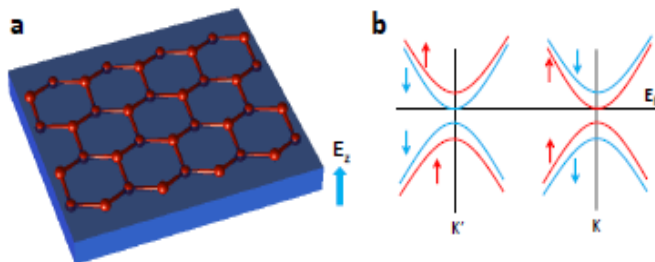
- Graphene-like two-dimensional silicon
- A finite band gap, be more compatible with existing silicon-based electronics
- Potential application as a high-performance field effect transistor



Nature, Scientific Reports 2, # 853, 2012

To grow **Silicene**, **Germanine**, and even **Tinene** on insulating or semiconducting substrate.

Superconductivity predicted in alkaline or alkaline earth elements doped silicene (CaC_6 $T_c=13\text{K}$; CaSi_6 $T_c = ?$)

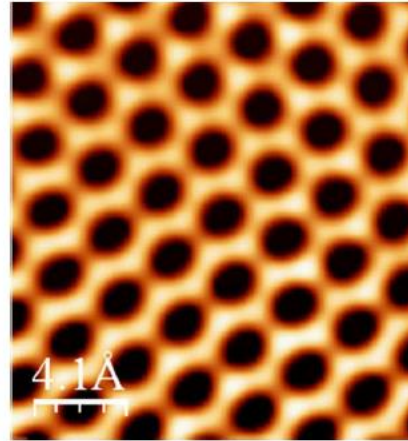


Silicene

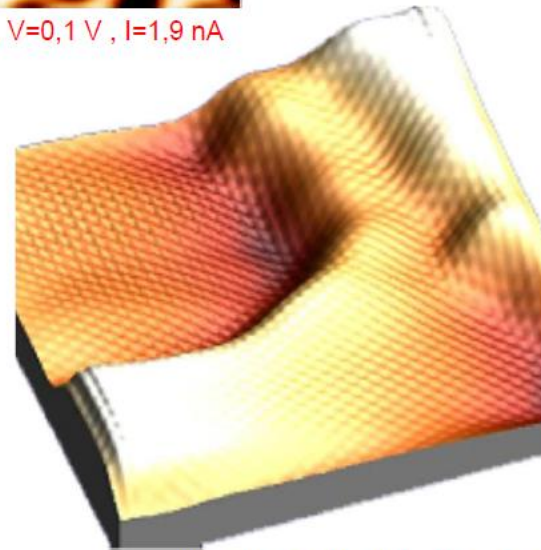
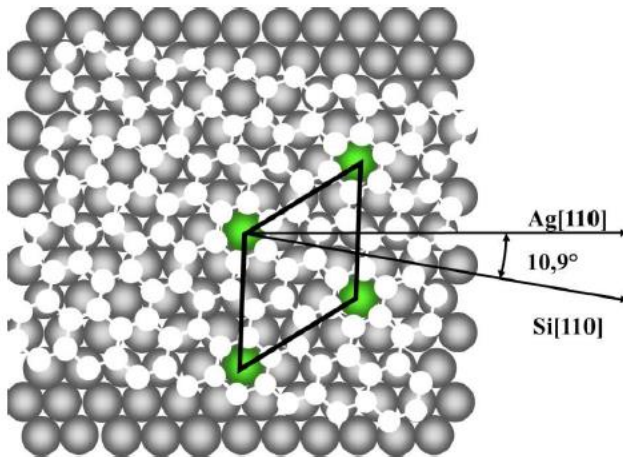
- Via deposition of Si on Ag (111) at 450K -500K.
- See B. Lalmi, APL (2010), and more.
- A buckled structure with a small gap of ~ 1.5 mV

Si/Ag(111)

$(2\sqrt{3} \times 2\sqrt{3})R30^\circ$



$22 \times 22 \text{ nm}^2$, $V=0,1 \text{ V}$, $I=1,9 \text{ nA}$



B. Lalmi et al, APL, 97, 223109 (2010)

Electronic properties (HRPES)

(4x4) superstructure

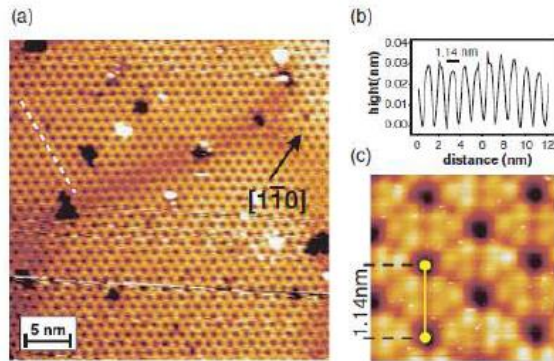


FIG. 2 (color). (a) Filled-states STM image of the 2D Si layer on Ag(111)-(1 × 1) ($U_{\text{bias}} = -1.3$ V, $I = 0.35$ nA). Clearly visible is the honeycomblike structure. (b) Line profile along the dashed white line indicated in (a). The dark centers in the STM micrograph are separated by 1.14 nm, corresponding to 4 times the Ag(111) lattice constant, in agreement with the (4×4) symmetry. (c) High-resolution STM topograph (3×3 nm, $U_{\text{bias}} = -1.3$ V, $I = 0.35$ nA) of the Si adlayer.

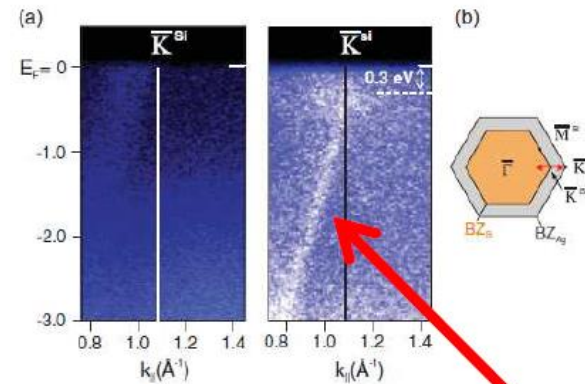


FIG. 3 (color). (a) ARPES intensity map for the clean Ag surface (left) and after formation of the 2D Si adlayer (right), taken along the Ag $\bar{\Gamma}$ - \bar{K} direction through the silicene \bar{K} ($h\nu = 126$ eV). (b) Brillouin-zone (BZ) scheme of the 2D Si layer with respect to the Ag(111)-(1 × 1) surface. The red arrow indicates the ARPES measurement direction.

Linear dispersion

PHYSICAL REVIEW B 87, 245430 (2013)

Absence of a Dirac cone in silicene on Ag(111): First-principles density functional calculations with a modified effective band structure technique

Yun-Peng Wang and Hai-Ping Cheng*

Quantum Theory Project and Department of Physics, University of Florida, Gainesville, Florida 32611, USA

(Received 22 February 2013; revised manuscript received 3 April 2013; published 24 June 2013)

We investigate the currently debated issue of the existence of the Dirac cone in silicene on an Ag(111) surface, using first-principles calculations based on density functional theory to obtain the band structure. By unfolding the band structure in the Brillouin zone of a supercell to that of a primitive cell, followed by projecting onto Ag and silicene subsystems, we demonstrate that the Dirac cone in silicene on Ag(111) is destroyed. Our results clearly indicate that the linear dispersions observed in both angular-resolved photoemission spectroscopy [P. Vogt *et al.*, *Phys. Rev. Lett.* **108**, 155501 (2012)] and scanning tunneling spectroscopy [L. Chen *et al.*, *Phys. Rev. Lett.* **109**, 066804 (2012)] come from the Ag substrate and not from silicene.

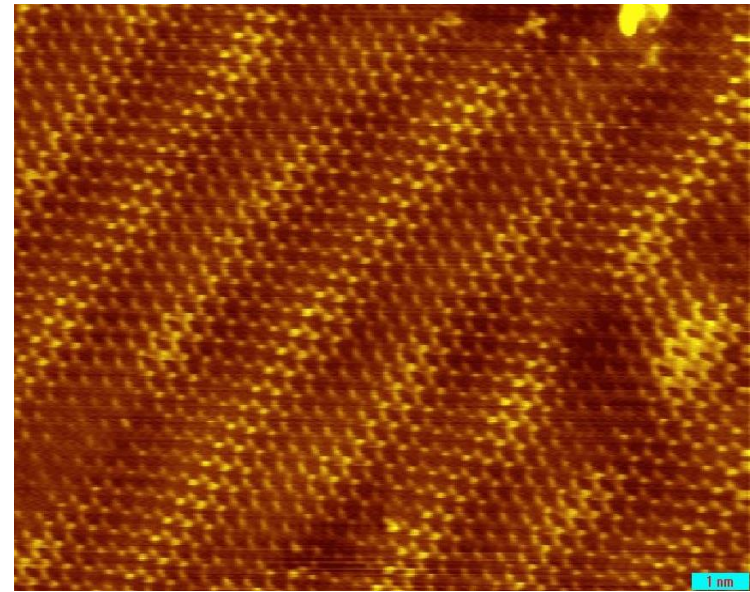
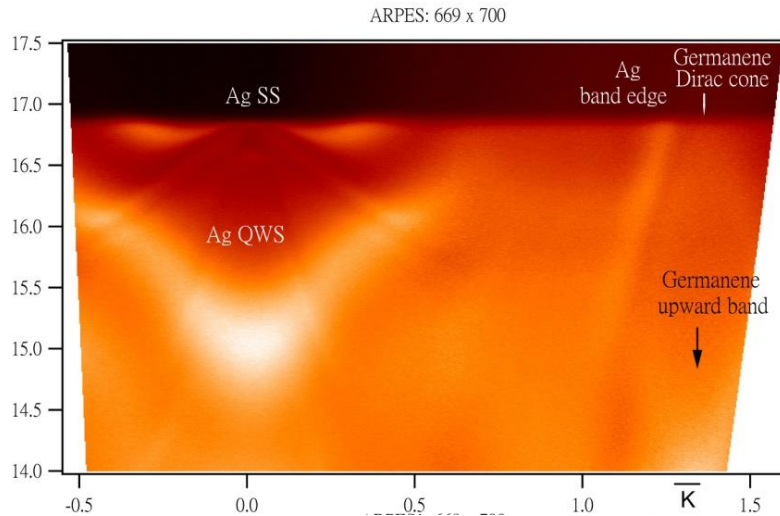
No Dirac cone

???

Y. Peng et al. Phys. Rev. B. 87 245430 (2013)

Demonstration of Germanene:

Germanene grown on Pb (111) on Ge (111)



First observation of Dirac cone

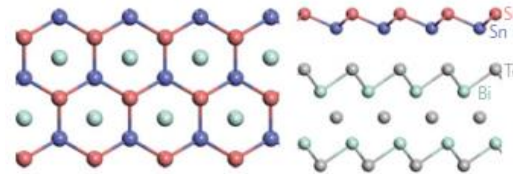
First observation of “real” Honeycomb

Prof. Shu-jung Tang et al, NTHU, 2015

Stanene

- Tin (*Sn*), not only for its large spin-orbit coupling, but for its integrability with conventional semiconductor industry.
 - ✓ With its elemental nature, Sn is free from the stoichiometry and related defects.
 - ✓ *Sn* is commonly used in many group-IV MBE system and is easy to tackle.
 - ✓ offers rich structures with different band diagrams from 3-D TI to 2-D TI.

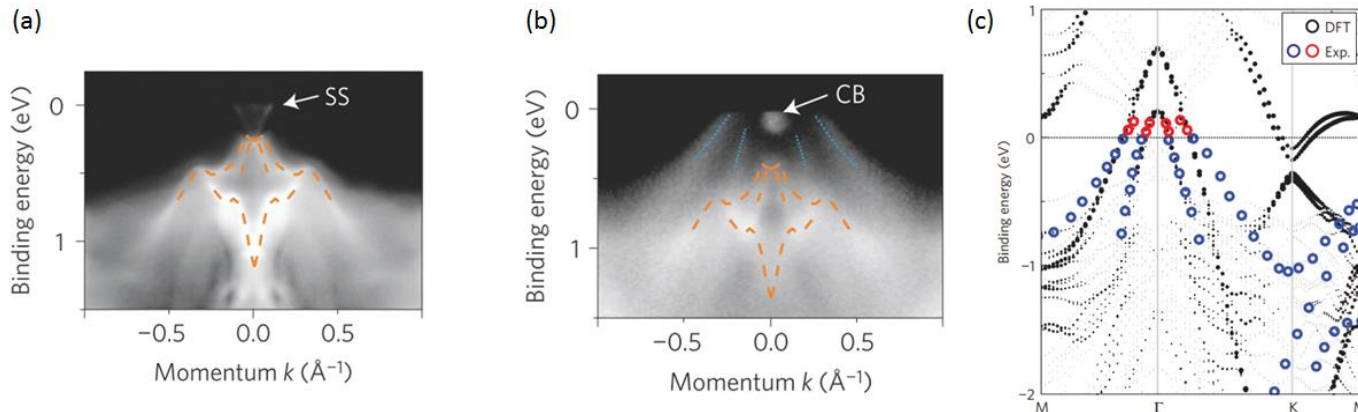
- stanene/ Bi_2Te_3 crystal structure



- **α -phase Sn** film was grown on *InSb*(001) as a 3-D TI, with nearly massless electron dispersion with a bandgap of **230 mV** showing spin helical band by ARPES.
- One monolayer (111)-orientated α -phase *Sn* is a buckled-honeycomb structure, similar to graphene.
- In this 2-D materials, stanene is special due to its outstanding properties : The Fermi velocity near Dirac point approaches 7.3×10^5 m/s, much larger than that of typical 3-D TI, and close to that of graphene (1×10^6 m/s).
- *Stanene could support a large-gap 2-D quantum spin Hall (QSH) state and thus enable the dissipationless electric conduction at RT.*

Stanene grown on $\text{Bi}_2\text{Te}_3(111)$

- Monolayer stanene was fabricated by MBE on $\text{Bi}_2\text{Te}_3(111)$ substrate.
- **Obvious discrepancies** :
First, according to ARPES spectra, the valence bands of stanene are pinned in the conduction band of $\text{Bi}_2\text{Te}_3(111)$, giving metallic interface states. **The inverted-bandgap at Γ point, as the key to QSH state, was not obtained.**
- **Second**, Dirac-cone-like features at K point are expected in a honeycomb structure; Stanene, with a larger SOC, leads to a bandgap of 0.1 eV at the Dirac-cone. **However, Dirac-cone at the K-point of stanene / $\text{Bi}_2\text{Te}_3(111)$ was not obtained.**



F. Zhu *et al.*
Nature Materials, **14**,
1020–1025 (2015).

(a) ARPES spectra of $\text{Bi}_2\text{Te}_3(111)$ (b) stanene on Bi_2Te_3 along K- Γ -K direction. The orange dashed lines mark the bulk band dispersions of Bi_2Te_3 . The blue dotted lines mark the hole band of stanene. SS marks the surface state and CB marks the conduction band of Bi_2Te_3 . (c) Comparison of experimental results with DFT calculation of stanene/ Bi_2Te_3 . Red dots above the Fermi level are obtained by in-situ potassium deposition that provides the film with electrons.